Electronic Supplementary Information

Two-Photon Induced Isomerization through a Cyaninic Molecular Antenna in Azo Compounds

Table of Contents

Table of figures

Experimental Procedures and Additional Experiments

General

IR spectra were acquired on a Perkin-Elmer Spectrum 100 FT-IR spectrometer. NMR spectra were obtained on a Bruker Avance 300 spectrometer, operating at a frequency of 300 MHz for ^{1}H and 75 MHz for ^{13}C on a Bruker Avance III HD 700 spectrometer operating at a 1H frequency of 699.95 MHz and 176MHz for ^{13}C. We used tetramethylsilane (TMS) as internal reference and $CDCl_3$, CD_2Cl_2, and DMSO-*d6* as solvent according to sample solubility. NMR spectra for the observation of the *cis* isomers and in following the *cis-to-trans* thermal relaxation were obtained on a Bruker Avance III HD 700 spectrometer operating at a 1H frequency of 699.95 MHz This spectrometer is equipped with a 5-mm z-axis gradient TCI cryoprobe. For these spectra we used deuterated acetonitrile as solvent (CD_3CN). Mass spectra were obtained on a JEOL JMSAX505 spectrometer. The values of the signals are expressed in mass/charge units (*m/z*), followed by the relative intensity with reference to a 100% base peak. Elemental analysis by combustion was performed in a Thermo Scientific Flash 2000 at 950°C. Methionine was used as a verification standard.

4-Iodoaniline, *N*-Methyl-*1H*-pyrrole, 4-hidroxyaldehyde, triethylamine, Potassium terbutoxide 1M in THF, Ph_3PCH_3Br and IR780 iodide, were purchased from SigmaAldrich and used without further purification. The [Pd(N,N)-pyrrole ligand] catalyst was synthetized according to a literature procedure[1].

Steady State and Femtosecond Resolved Spectroscopies

UV-Vis absorption spectra were recorded in a Cary 50 spectrometer, fluorescence spectra and fluorescence quantum yields were measured in a Varian Cary Eclipse fluorimeter. The solvent used for all experiments was acetonitrile HPLC grade and was acquired from Sigma Aldrich. For the study of the excited state dynamics with two-photon (860 nm) excitation, we employed the femtosecond fluorescence up-conversion technique. Our setup has been described in detail previously.[2–5] Briefly, the pulsed light source was a regeneratively amplified Ti:Sapphire laser tuned at 860 nm. This wavelength was selected in order to guarantee two-photon excitation of the molecules of this study. Tuning to this frequency allows excitation into the higher singlet states in the 430 nm region of the IR780 cyanine or the polymethinic section of Cy-SAP. The laser produced a 1 kHz pulse train with a temporal width of 100 fs and up to 0.8 mJ per pulse. The intensity at the samples was modulated with beamsplitters and a variable neutral optical density filter.

The spontaneous emission from the higher states of the molecules of this study was collected and refocused by a pair of parabolic mirrors, and the residual excitation radiation was removed by a long or short pass filter. The emission was focused into a Type I β-BBO crystal making a small angle respect to the gate-pulse which was previously separated from the fundamental beam and delayed with a translation state. The polarization of the excitation pulse for the time resolved emission spectra was set to the magic angle (54.7°) respect to the non-linear crystal acceptance direction (vertical). The up-conversion signal was focused into a double monochromator (Oriel) and detected with a photomultiplier tube connected to a lock-in amplifier (Stanford Research Systems) which was referenced to the third sub-harmonic of the laser repetition rate. The instrument response function (IRF) for the up-conversion system was determined to be Gaussian with a FWHM of 260 fs. This was determined from the instrument-limited emission signal rise of coumarin-102 at 460 nm. For the up-conversion experiments, the solutions of Cy-SAP, SAP and IR780 were kept flowing through a 1 mm quartz cell. For the anisotropy measurements, the polarization of the excitation beam was adjusted before the sample so that the parallel or perpendicular component of the fluorescence was up-converted at the crystal.

Detailed Synthetic Procedures and Characterization

(E)-2-((4-iodophenyl)diazenil)-N-Methyl-1H-pyrrole – (5)

A 250 ml round-bottomed flask, equipped with a magnetic stir bar, was charged with acetone (15 ml), water (15 ml) and 4-Iodoaniline (2.1 g, 9.6 mmol, 1.2 eq.). The resulting mixture was cooled to 0°C and 12M HCl solution was added slowly into the mixture (13 ml, 164 mmol, 20.5 eq.). Next, a $NaNO_2$ solution (0.77 g, 10.64 mmol, 1.4 eq. in 5 ml of water) was added dropwise. After an hour, a mixture of acetone (15 ml), water (15 ml), N-Methyl-1H-pyrrole (0.65 g, 8.0 mmol, 1.0 eq.) and Na_2CO_3 (1.7 g, 16 mmol, 2.0 eq), was transferred slowly into the flask. The mixture was left stirring for another hour.

Then, the acetone was removed in vacuum. Next, the aqueous phase was extracted three times with DCM (50 ml) and the organic phase was dried over anhydrous Na_2SO_4. The crude material was purified by column chromatography on silica gel eluting with 5-30% ethyl acetate in hexane to give **5** (2.47g, MW= 311.12 g/mol, 7.9mmol, 99%) as an orange solid.

^{1}H NMR (300 MHz, DMSO-d6) δ 7.99 – 7.77 (m, 2H), 7.63 – 7.48 (m, 2H), 7.33 (t, J = 2.1 Hz, 1H), 6.65 (dd, J = 4.2, 1.7 Hz, 1H), 6.31 (dd, J = 4.2, 2.6 Hz, 1H), 3.92 (s, 3H).

HRMS [ESI+]: calculated for $C_{11}H_{11}IN_3$ $[M+H]^+$: 311.99976, found: 311.99977. Mass diff. (ppm)= 0.01

4-Vinylphenol – (7)

In a round-bottomed flask, Ph_3PCH_3Br (5.5 g, 15 mmol, 1.5 eq.) was set at N_2 atmosphere. Next, a solution of t-BuOK in THF (1M, 25 ml, 25 mmol, 2.5 eq.) was poured over and left stirring at room temperature for 10 minutes. Then, 4-hidroxyaldehyde (1.3g, 10.6 mmol, 1.0 eq.) was added and left for 24h at room temperature. The reaction was quenched with 100 ml of saturated NH_4Cl water solution. The aqueous phase was extracted three times with DCM (50 ml). The organic phase then is washed with brine to remove any salt left and dried over anhydrous Na_2SO_4. The crude product was purified with column chromatography on silica gel eluting with 10% ethyl acetate in hexane to give **7** (1.11g, MW=120.15 g/mol, 9.2 mmol, 86.7%) as a white solid.

^{1}H NMR (700 MHz, DMSO-d6): 9.51 (s, 1H), 7.49 – 7.14 (m, 2H), 6.74 (dd, J = 8.5, 1.5 Hz, 2H), 6.61 (dd, J = 17.6, 10.9 Hz, 1H), 5.58 (dd, J = 17.6, 1.1 Hz, 1H), 5.04 (dd, J = 10.9, 1.1 Hz, 1H).

HRMS [ESI+]: calculated for $C_8H_9O_1$ $[M+H]^+$: 121.06534, found: 121.06527. Mass diff. (ppm)= -0.60

SAP: 4-((E)-4-((E)-(1-methyl-1H-pyrrol-2-yl)diazenyl)styryl)phenol – (1)

A round-bottomed flask was charged with **7** (0.83 g, 6.9 mmol, 1.2 eq), **5** (1.7 g, 5.4 mmol, 1.0 eq), triethylamine (1.82 ml, 10.8 mmol, 2.0 eq), DMF (60 ml) and [Pd(N,N)-pyrrole ligand] catalyst solution (3.6mM in DMF, 3.5 ml, 0.1%). The mixture was stirred at reflux for 2 hours. After cooling, 40 ml of NH_4Cl saturated solution was added. The mixture was extracted with DCM 3x50ml and the organic phase was thoroughly washed with brine to remove the excess DMF and then, was dried over anhydrous Na_2SO_4. The mixture was purified by column chromatography on silica gel eluting with 5-50% ethyl acetate in hexane to give **1** (1.31 g, MW=303.36 g/mol, 4.32 mmol, 77.4%) as a dark orange solid.

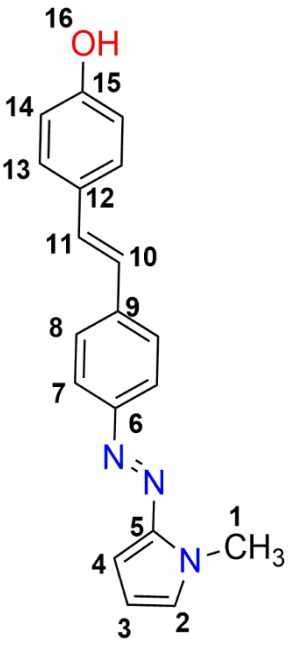

^{1}H NMR (300 MHz, DMSO-d_6): 9.64 (s, 1H, H_{16}), 7.75 (d, *J* = 8.6 Hz, 2H, H_7), 7.66 (d, *J* = 8.6 Hz, 2H, H_8), 7.50 – 7.41 (m, 2H, H_{13}), 7.30 – 7.17 (m, 2H, H_2, H_{11}), 7.08 (d, *J* = 16.4 Hz, 1H, H_{10}), 6.85 – 6.74 (m, 2H, H_{14}), 6.59 (dd, *J* = 4.1, 1.6 Hz, 1H, H_4), 6.29 (dd, *J* = 4.2, 2.6 Hz, 1H, H_3), 3.93 (s, 3H, H_1). **^{13}C NMR** (75 MHz, DMSO-d_6) δ 157.60 (C_{15}), 151.84 (C_6), 146.06 (C_5), 138.89 (C_9), 129.62 (C_{11}), 128.21 (C_{12}), 128.13 (C_{13}), 128.01 (C_2), 126.82 (C_8), 124.43 (C_{10}), 122.13 (C_7), 115.62 (C_{14}), 110.17 (C_3), 99.61 (C_4), 33.06 (C_1). **^{1}H, ^{13}C-HSQC** (300 MHz / 75 MHz, DMSO-d_6): δ(^{1}H) / δ(^{13}C) = 3.93/32.66 (H_1/ C_1), 6.29/109.85 (H_3/ C_3), 6.60/99.10 (H_4/ C_4), 6.79/115.14 (H_{14}/ C_{14}), 7.12/124.02, 7.05/123.96 (H_{10}/ C_{10}), 7.22/129.05, 7.28/128.98 (H_{11}/ C_{11}), 7.27/127.90 (H_2/ C_2), 7.46/127.76 (H_{13}/ C_{13}), 7.67/126.60 (H_8/ C_8), 7.74/121.61 (H_7/C_7). **^{1}H, ^{13}C-HMBC** (300 MHz / 75 MHz, DMSO-d_6): δ(^{1}H) / δ(^{13}C) = 3.94/ 128.69, 146.55 (H_1/ $C_{2,5}$), 6.30/100.06 (H_3/ C_4), 6.60/110.64 (H_4/ C_3), 6.80/116.09, 128.47, 158.02 (H_{14}/ $C_{14,12,15}$), 7.10,7.04/ 138.93, 129.67, 127.11 (H_{10}/ $C_{9,11,12}$), 7.22,7.27/ 124.43, 128.21, 138.93 (H_{11}/ $C_{10,12,9}$), 7.27/ 99.61, 110.17,146.06 (H_2/ $C_{4,3,5}$), 7.45/ 156.97, 128.11 (H_{13}/ $C_{15,13}$), 7.66/ 124.29, 126.77,151.77 (H_8/ $C_{10,8,6}$), 7.76/ 122.03, 138.80 (H_7/ $C_{7,9}$),**IR** (KBr) v max 3223.73, 3017.84, 2921.32, 1585.35, 1507.37, 1470.79, 1392.32, 1350.68, 1324.78, 1241.87, 1166.83, 1042.97, 959.76, 834.20, 719.73, 539.73. **HRMS** [ESI+]: calculated for $C_{19}H_{18}N_3O$ $[M+H]^+$: 304.14499, found: 304.14357. Mass diff. (ppm)= -4.65. **EA:** Calculated: 13.85% N, 75.23% C, 5.65%, found 13.04% N, 73.53 % C, 5.45 % H.

Cy-SAP: 2-((E)-2-((E)-3-((E)-2-(3,3-dimethyl-1-propylindolin-2-ylidene)ethylidene)-2-(4-((E)-4-((E)-(1-methyl-1H-pyrrol-2-yl)diazenyl)styryl)phenoxy)cyclohex-1-en-1-yl)vinyl)-3,3-dimethyl-1-propyl-3H-indol-1-ium iodide. – (2)

In an amber round-bottomed flask, IR780-I (0.71g, 1.1 mmol, 1.0 eq.), **1** (2.68g, 2.7 mmol, 2.5 eq.), triethylamine (8.2 ml, 58.9 mmol, 55 eq.) and MeCN anhydrous (80 ml) were charged, then left stirring 24h at room temperature. Then, after the temperature was raised to 40 °C for 2h, the solvents are evaporated in vacuum. The compound **1** was thoroughly removed by two consecutive silica gel column chromatography, using DCM/EtOH (100% →50:50). The crude was purified further by recrystallization by slow diffusion of diethyl ether to a saturated DCM solution. A dark green solid was obtained, which was extensively washed with diethyl ether. The solid was identified as **2** (765.8 mg, MW=934.00 g/mol, 0.82 mmol, 74.5%).

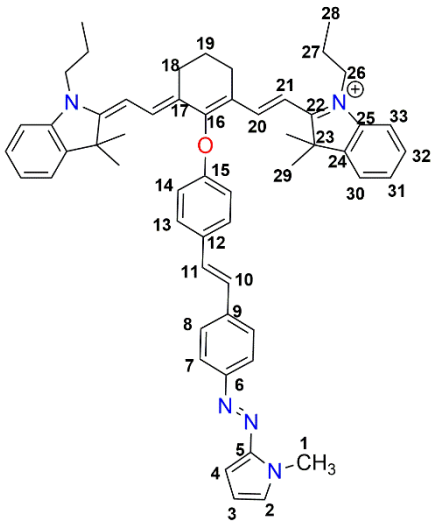

^{1}H NMR (700 MHz, CD_2Cl_2): 7.96 (d, J = 14.1 Hz, 2H, H_{20}), 7.85 – 7.74 (m, 2H, H_8), 7.65 – 7.55 (m, 4H, H_{14}, H_7), 7.36 (td, J = 7.7, 1.2 Hz, 2H, H_{32}), 7.30 (dd, J = 7.6, 1.2 Hz, 2H, H_{30}), 7.20 (td, J = 7.5, 0.9 Hz, 2H, H_{31}), 7.16 (d, J = 16.3 Hz, 1H, H_{11}), 7.14 – 7.10 (m, 4H, H_{13}, H_{33}), 7.09 (d, J = 16.4 Hz, 1H, H_{10}), 6.98 (dd, J = 2.6, 1.7 Hz, 1H, H_2), 6.65 (dd, J = 4.2, 1.7 Hz, 1H, H_4), 6.28 (dd, J = 4.2, 2.6 Hz, 1H, H_3), 6.04 (d, J = 14.2 Hz, 2H, H_{21}), 3.99 (t, J = 7.9, 7.3 Hz, 4H, H_{26}), 3.95 (s, 3H, H_1), 2.73 (t, J = 6.3 Hz, 4H, H_{18}), 2.06 (q, J = 6.3 Hz, 2H, H_{19}), 1.86 (h, J = 7.4 Hz, 4H, H_{27}), 1.37 (s, 12H, H_{29}), 1.04 (t, J = 7.4 Hz, 6H, H_{28}). **^{13}C NMR** (176 MHz, CD_2Cl_2): 172.86 (C_{22}), 164.72 (C_{16}), 160.19 (C_{15}), 153.47 (C_6), 147.26 (C_5), 142.82 (C_{20}), 142.70 (C_{25}), 141.61 (C_{24}), 138.84 (C_9), 132.43 (C_{12}), 129.10 (C_7), 129.06 (C_{32}), 128.76 (C_{11}), 127.79 (C_{10}), 127.51 (C_2), 127.44 (C_{14}), 125.57 (C_{31}), 122.96 (C_8), 122.72 (C_{30}), 122.54 (C_{17}), 115.64 (C_{13}), 111.19 (C_{33}), 110.74 (C_3), 100.38 (C_{21}), 100.30 (C_4), 49.62 (C_{23}), 46.50 (C_{26}), 33.81 (C_1), 28.24 (C_{29}), 24.94 (C_{18}), 21.70 (C_{19}), 21.26 (C_{27}), 11.88 (C_{28}). **^{1}H, ^{1}H-COSY** (700 MHz / 700 MHz, CD_2Cl_2): δ(^{1}H) / δ(^{1}H) = 1.08/1.88 (H_{28}/ H_{27}), 1.88/4.02 (H_{27}/ H_{26}), 2.10/2.76 (H_{19}/ H_{18}), 6.07/8.00 (H_{21}/ H_{20}), 6.32/6.68, 7.02 (H_3/ H_4, H_2,), 7.62/7.16 (H_{14}/ H_{13},), 7.62/7.82 (H_7/ H_8), 7.16/7.40 (H_{33}/ H_{32}).**^{1}H, ^{13}C-HSQC** (700 MHz / 176 MHz, CD_2Cl_2): δ(^{1}H) / δ(^{13}C) = 1.04/11.29 (H_{28}/ C_{28}),1.37/27.67 (H_{29}/ C_{29}), 1.86/20.66 (H_{27}/ C_{27}), 2.07/21.13 (H_{19}/ C_{19}), 2.73/24.40 (H_{18}/ C_{18}), 3.96/33.05 (H_1/ C_1), 3.99/45.90 (H_{26}/ C_{26}), 6.05/99.80 (H_{21}/ C_{21}), 6.28/110.01 (H_3/ C_3), 6.65/99.50 (H_4/ C_4), 6.98/127.02 (H_2/ C_2), 7.07/127.15 (H_{10}/ C_{10}), 7.11/110.62 (H_{33}/ C_{33}), 7.13/115.05 (H_{13}/ C_{13}), 7.15/128.08 (H_{11}/ C_{11}), 7.20/124.98 (H_{31}/ C_{31}), 7.29/122.17 (H_{30}/ C_{30}), 7.36/128.53 (H_{32}/ C_{32}), 7.59/127.88 (H_{14}/ C_{14}, H_7/ C_7), 7.80/122.36 (H_8/ C_8), 7.97/142.22 (H_{20}/ C_{20}).**^{1}H, ^{13}C-HMBC** (700 MHz / 176 MHz, CD_2Cl_2): δ(^{1}H) / δ(^{13}C) = 1.04/20.68, 45.93 (H_{28}/ $C_{27,26}$), 1.37/27.65, 49.04, 141.03, 172.27 (H_{29}/ $C_{29,23,24,22}$), 1.86/11.29, 45.93 (H_{27}/ $C_{28,26}$), 2.06/24.36, 121.98 (H_{19}/ $C_{18,17}$), 2.73/24.26, 121.98, 142.13, 164.15 (H_{18}/ $C_{18,17,20,16}$), 3.95/127.21, 146.68 (H_1/ $C_{2,5}$), 3.99/11.29, 20.67,142.25,172.28 (H_{26}/ $C_{28,27,25,22}$), 6.04/49.04, 121.96, 142.01 (H_{21}/ $C_{23,17,20}$), 6.29/127.19, 146.70 (H_3/ $C_{2,5}$), 6.66/127.25, 146.70 (H_4/ $C_{2,5}$), 6.98/99.72,110.15, 127.28, 146.66 (H_2/ $C_{4,3,2,5}$), 7.08/127.21, 131.91 (H_{10}/ $C_{11,12}$), 7.11/124.92, 141.11 (H_{33}/ $C_{31,25}$),7.12/115.07, 131.87, 159.61 (H_{13}/ $C_{13,12,15}$), 7.15/128.12, 138.15 (H_{11}/ $C_{11,9}$), 7.20/110.62, 122.21, 141.11 (H_{31}/ $C_{33,30,24}$), 7.30/49.05, 128.53, 142.24 (H_{30}/ $C_{23,32,25}$), 7.36/110.64, 122.20, 142.18 (H_{32}/ $C_{33,30,25}$), 7.59/127.43, 159.62 (H_{14}/ $C_{14,15}$), 7.60/122.14,152.90 (H_7/ $C_{8,6}$), 7.96/24.35, 121.98, 164.15, 172.27 (H_{20}/ $C_{18,17,16,22}$).**IR** (KBr) vmax 2958.91, 2923.43, 2868.63, 1556.07, 1505.46, 1397.06, 1353.05, 1228.10, 1149.55, 1083.01, 1034.67, 993.80, 912.94, 788.72, 707.09. **HRMS** [FAB+]: calculated for $C_{55}H_{60}N_5O$ $[M]^+$: 806.4798, found: 806.4794. Mass diff. (ppm)= -0.5 **EA:** Calculated, 7.50% H, 70.73% C, 6.48% H; found, 7.14% N, 68.70% C, 6.40

NMR spectra of all compounds synthetized

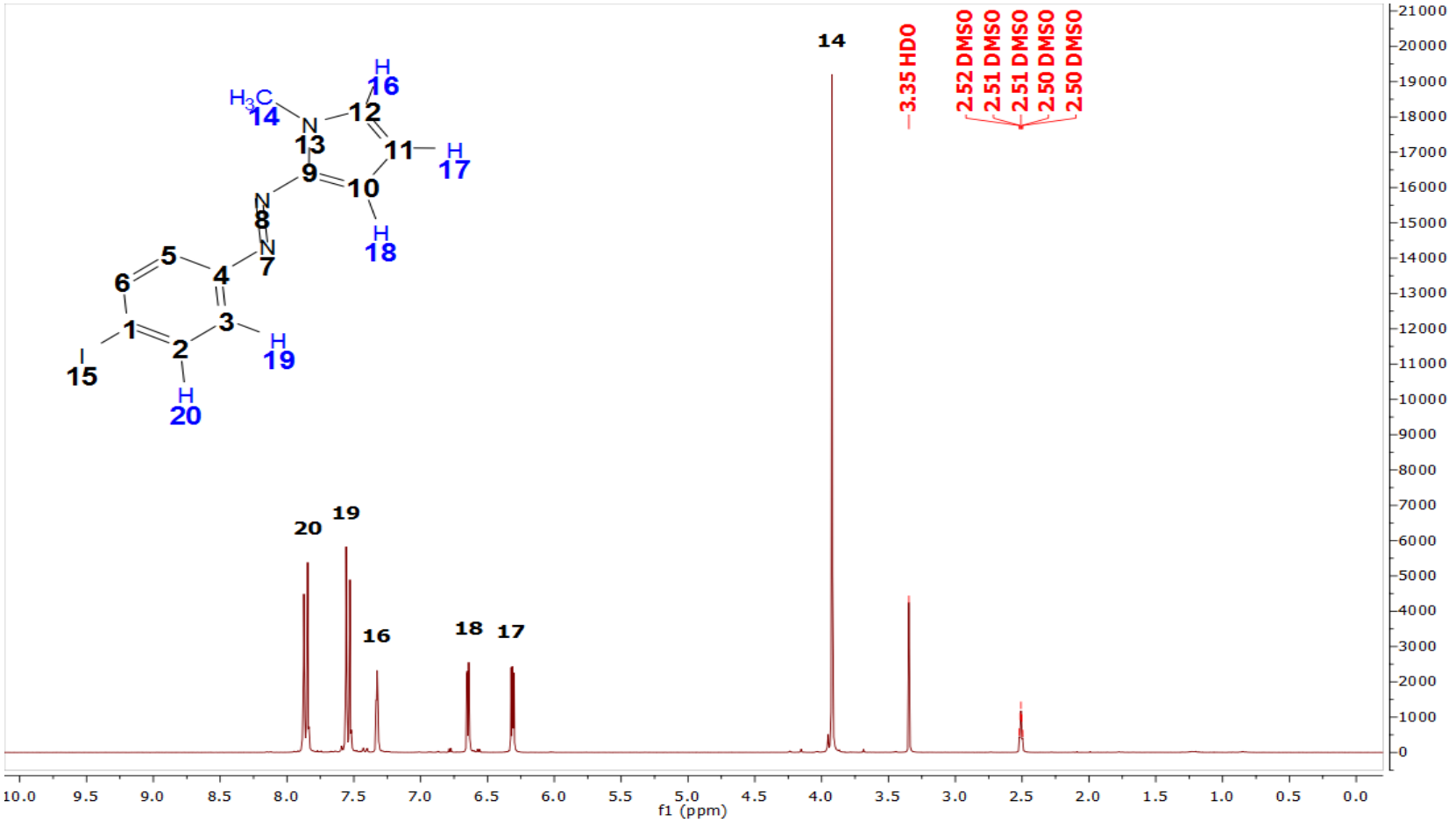

Figure S1. ^{1}H NMR (300 MHz, DMSO-d6) spectrum of (E)-2-((4-iodophenyl)diazenil)-N-Methyl-1H-pyrrole – (5).

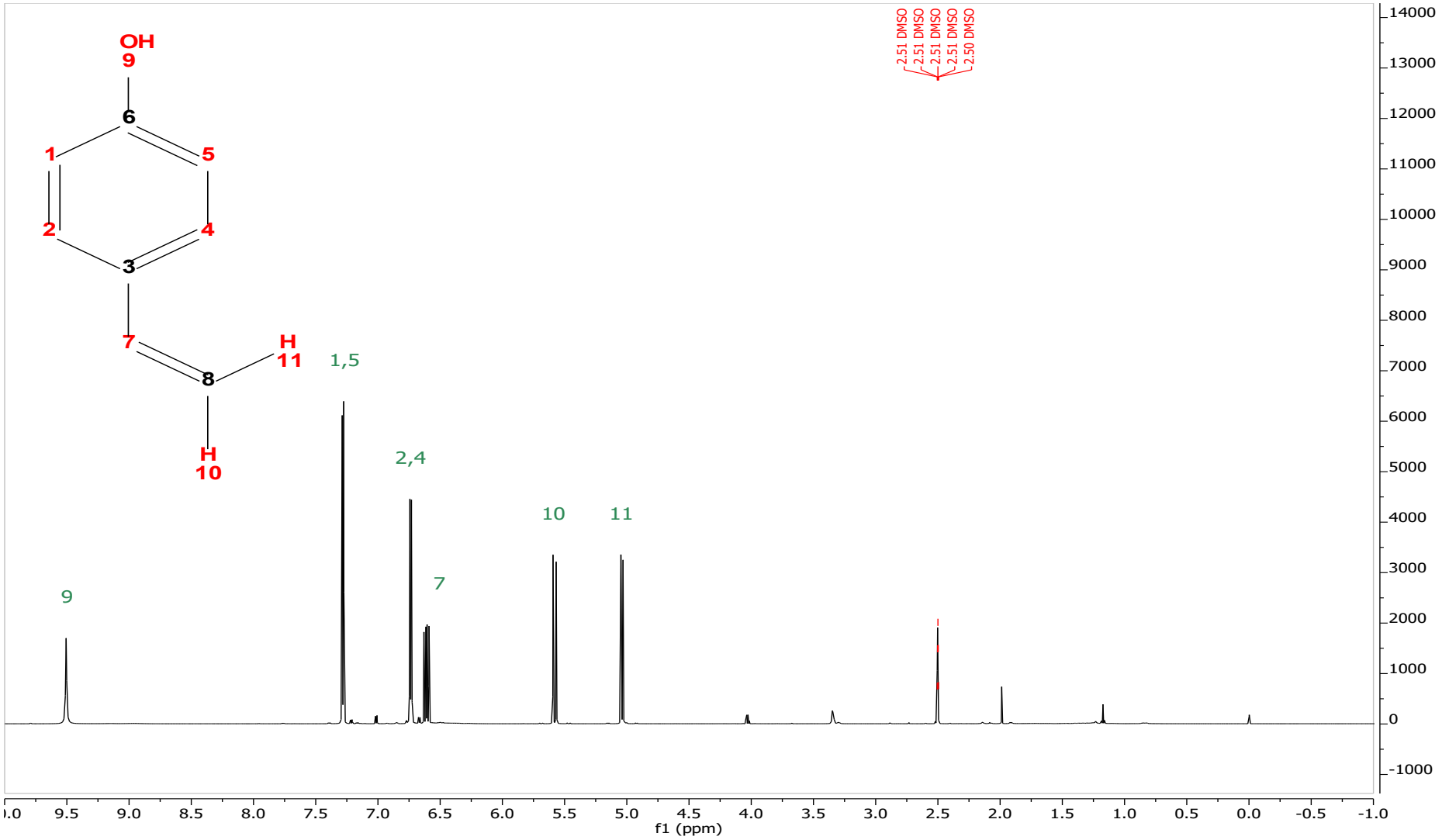

Figure S2. ^{1}H NMR (300MHZ, CDCl3) spectrum of 4-Vinylphenol – (7)

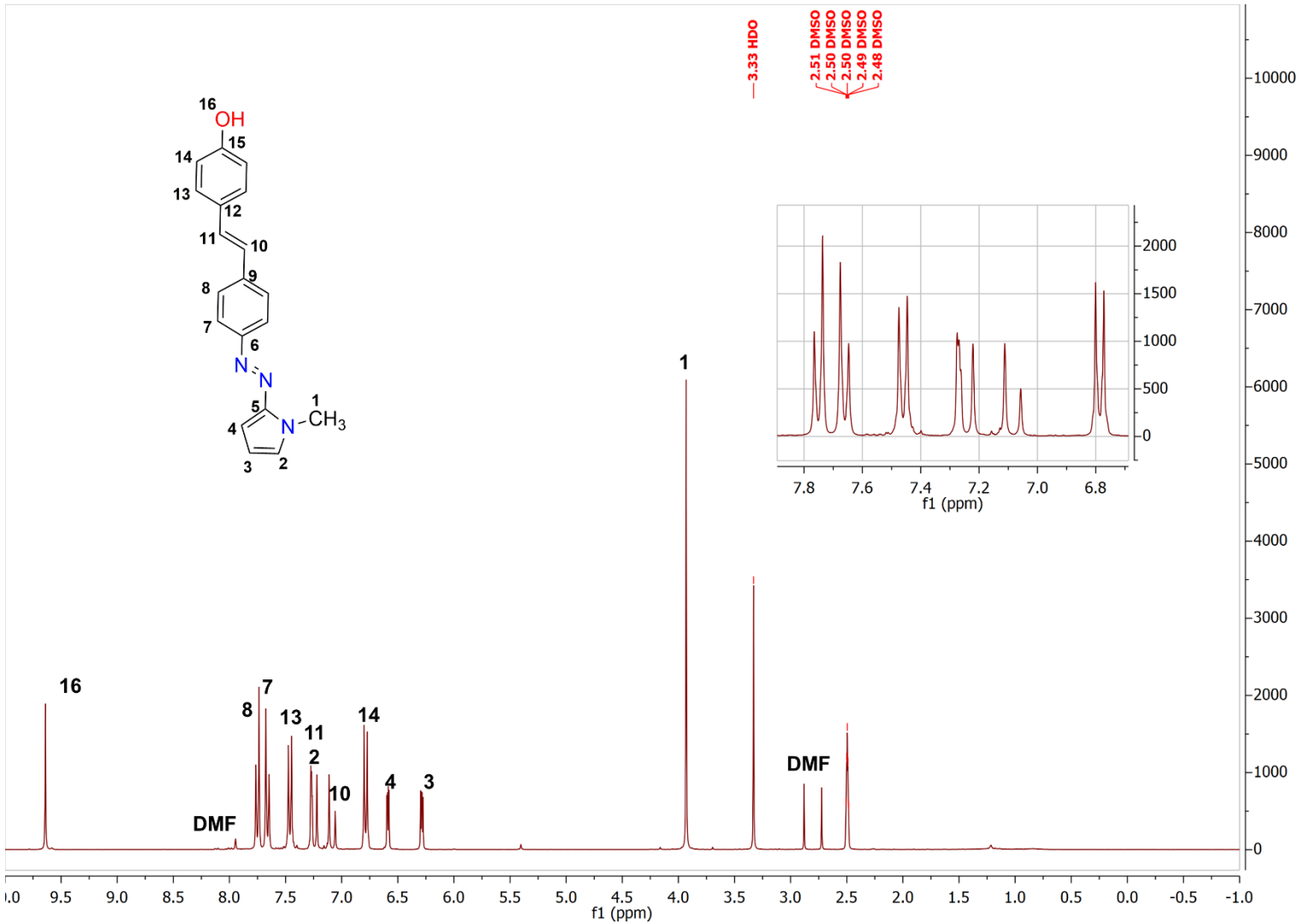

Figure S3. ^{1}H NMR (300 MHz, DMSO-d6) spectrum of SAP: 4-((E)-4-((E)-(1-methyl-1H-pyrrol-2-yl)diazenyl)styryl)phenol – (1). ^{1}H and ^{13}C chemical shifts are based on HSQC and HMBC NMR spectra. The signals assigned to residual DMF (2.7, 2.8, 7.9 ppm all singlets) are in accordance with values reported in the literature.[6]

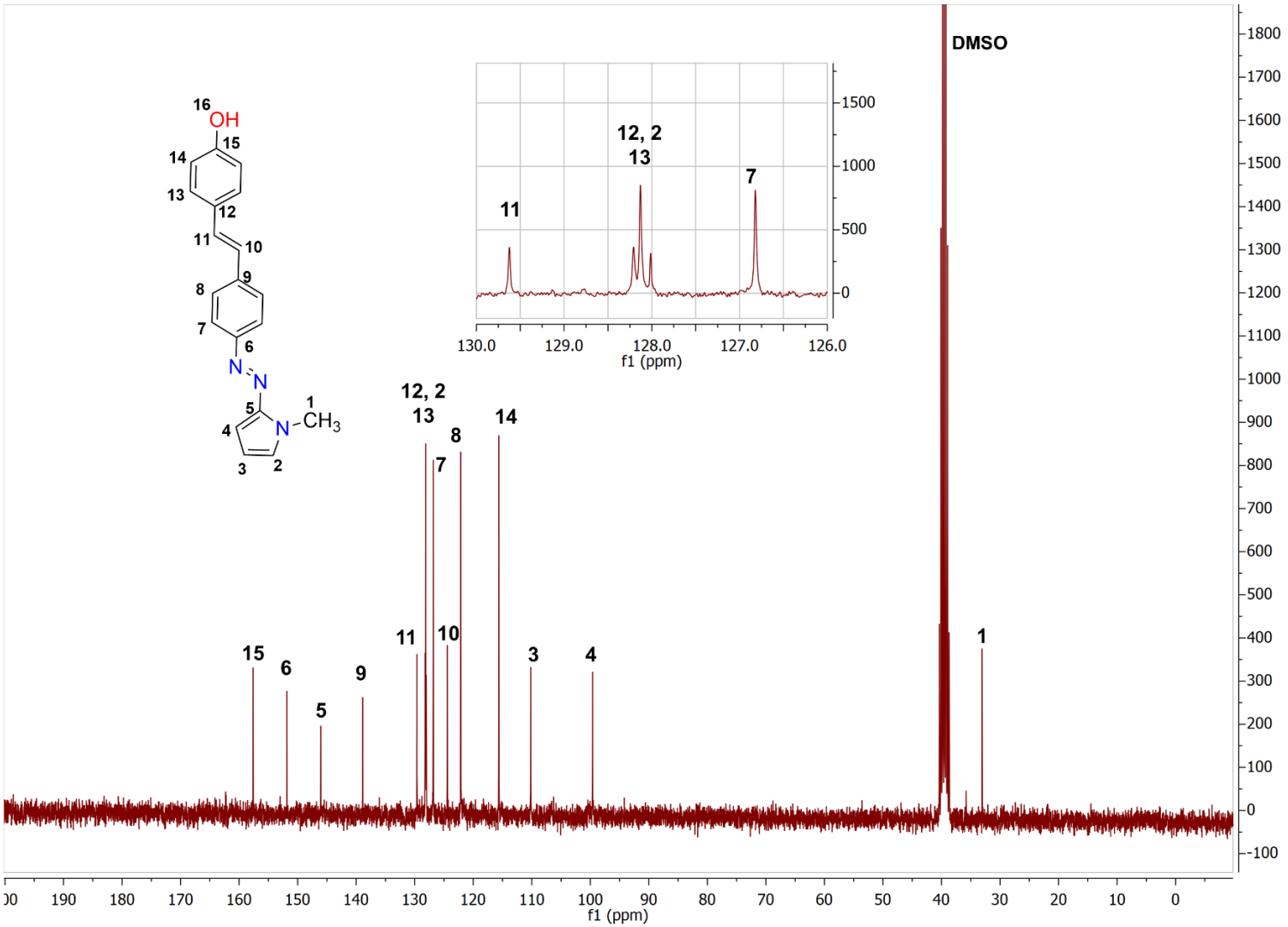

Figure S4. ^{13}C NMR (75 MHz, DMSO) spectrum of SAP: 4-((E)-4-((E)-(1-methyl-1H-pyrrol-2-yl)diazenyl)styryl)phenol – (1). The inset shows an expanded view of the signals crowded around 128 ppm. ^{1}H and ^{13}C chemical shifts are based on 2D HSQC, and HMBC NMR spectra.

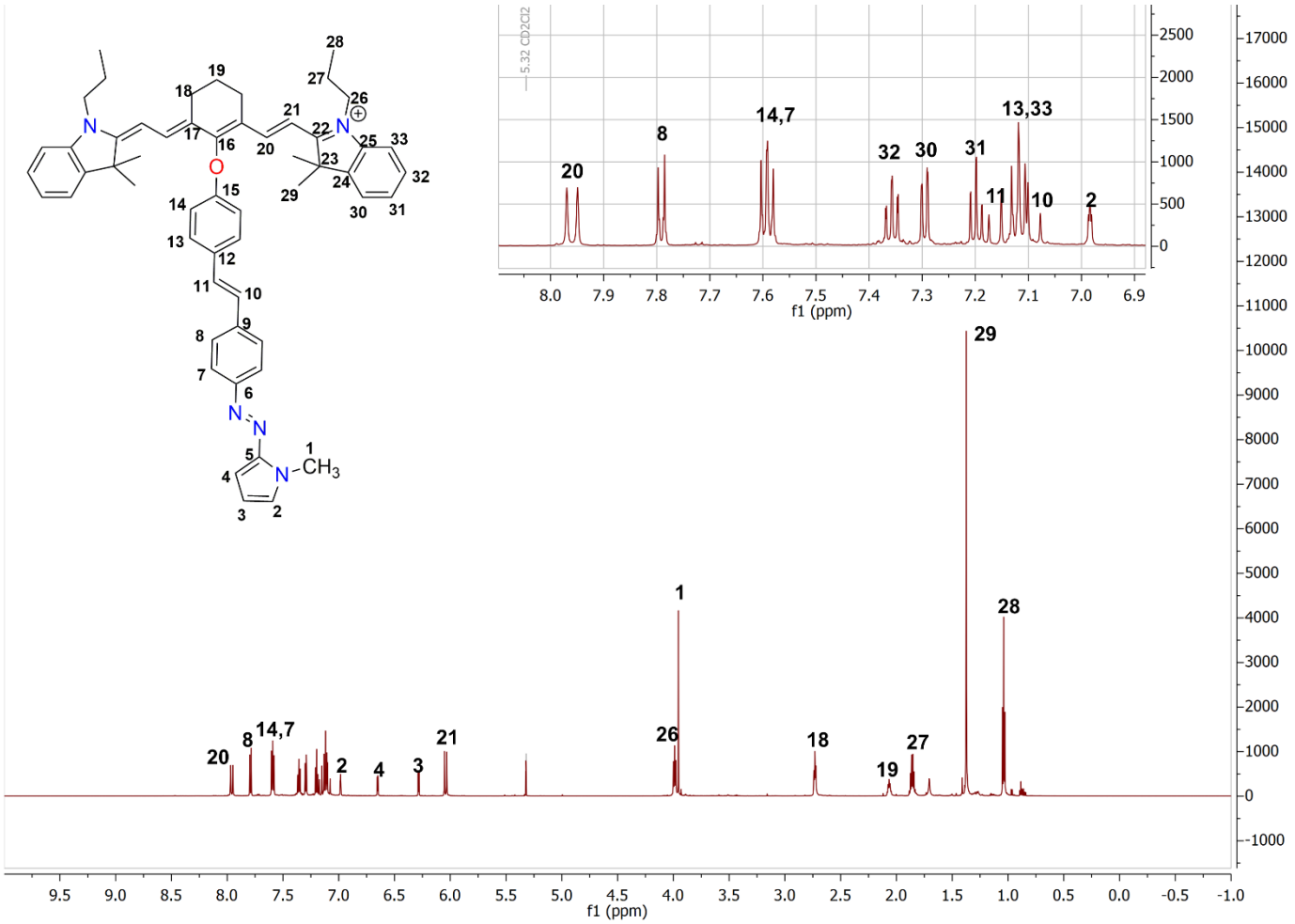

Figure S5. ^{1}H NMR (700MHz, CD_2Cl_2) spectrum of Cy-SAP: 2-((E)-2-((E)-3-((E)-2-(3,3-dimethyl-1-propylindolin-2-ylidene)ethylidene)-2-(4-((E)-4-((E)-(1-methyl-1H-pyrrol-2-yl)diazenyl)styryl)phenoxy)cyclohex-1-en-1-yl)vinyl)-3,3-dimethyl-1-propyl-3H-indol-1-ium iodide. – (2). ^{1}H and ^{13}C chemical shifts are based on 2D HSQC, HMBC and COSY NMR spectra. The inset shows an expanded view of signals crowded around 7.5 ppm.

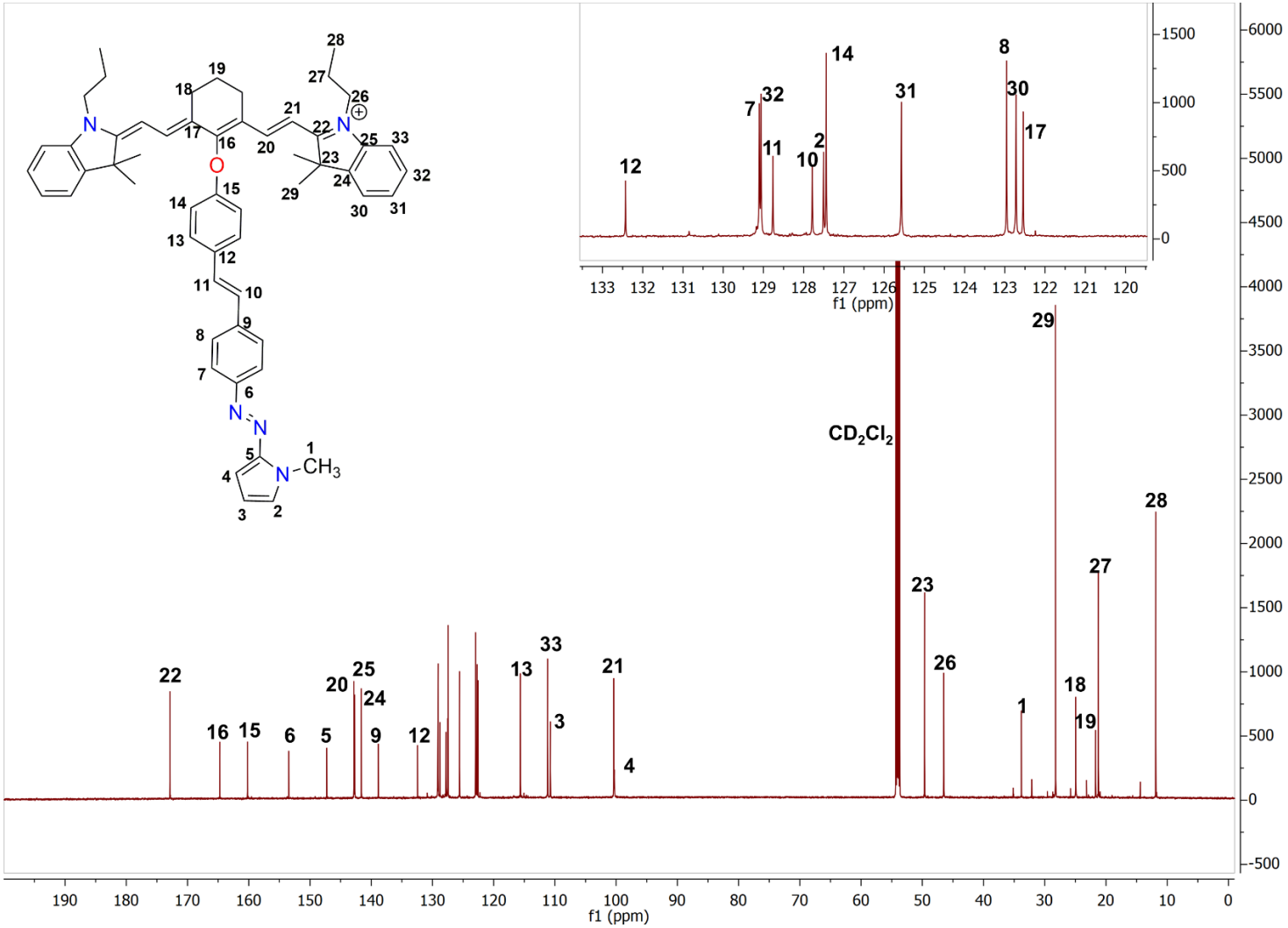

Figure S6. ^{13}C NMR (176 MHz, CD_2Cl_2) spectrum of Cy-SAP: 2-((E)-2-((E)-3-((E)-2-(3,3-dimethyl-1-propylindolin-2-ylidene)ethylidene)-2-(4-((E)-4-((E)-(1-methyl-1H-pyrrol-2-yl)diazenyl)styryl)phenoxy)cyclohex-1-en-1-yl)vinyl)-3,3-dimethyl-1-propyl-3H-indol-1-ium iodide. – (2). The inset shows an expanded view of signals crowded around 126 ppm. ^{1}H and ^{13}C chemical shifts are based on 2D HSQC, HMBC and COSY NMR spectra.

Steady State Spectroscopy from upper excited electronic states of the IR780 cyanine dye

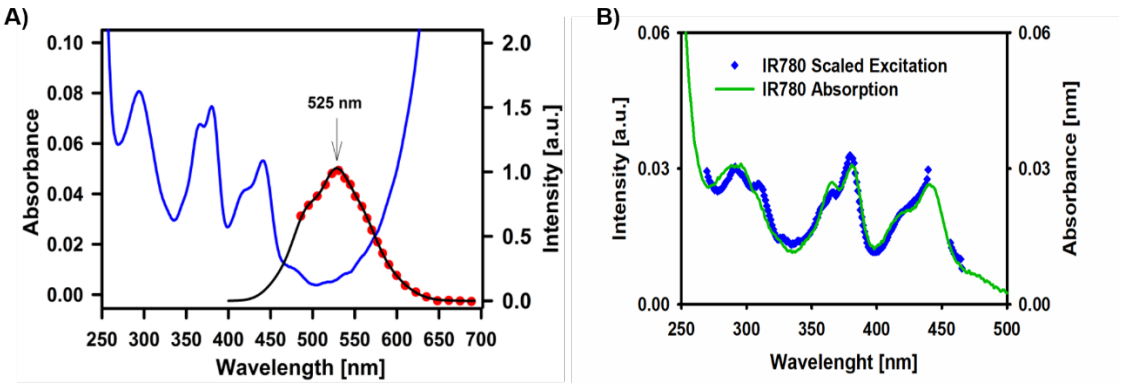

Figure S7. Steady state spectroscopy for the higher excited states (S_n, n>1) of the IR780 cyanine dye. A) Absorption spectrum (blue line). The corrected emission spectrum from the second excited singlet state is presented in red symbols. The black line corresponds to an estimation of the second singlet emission spectrum formed with a pair of log-normal functions. B) Absorption (green) and excitation (blue symbols) spectra of the IR780 cyanine in methylene chloride. The emission at 528 nm was monitored. All spectra were taken in acetonitrile. The missing blue symbols are due to the presence of a Raman band.

Computational Chemistry Methods

In order to determine the energy transfer parameters involved in the photoactivation of the Cy-SAP system, we performed DFT calculations using the Gaussian09-E0.1 set of programs[7] for the SAP and IR-780 molecules. In particular, the directions of the corresponding transition dipole moments are crucial to estimate the energy transfer efficiency as described in the manuscript. The ground state geometry optimizations and frequencies were obtained using the PBE0 and M06 hybrid functionals and the 6-311++G(d,p) basis set. These are among the best general purpose functionals for large organic molecule excited state calculations.[8–16] Our main use of these results is the estimation of the relative direction between the transition moment vectors relevant in the indirect excitation of the actuator section (from the higher cyanine-localized state to the excited state localized in the stilbenyl-azo section). The transition dipole moment vectors are important parameters which determine the efficiency of energy transfer. The calculations were carried out in solution (acetonitrile) with the polarizable continuum model (PCM). The absence of imaginary frequencies in these calculations confirmed the global energy minimum of the ground state equilibrium geometry. The excitation energies were corrected by state-specific solvation of the vertical excitation states.

The ground state equilibrium geometries were optimized using the PBE0 (PBE1PBE) and M06 as functionals, along with the base set 6-311++G(d,p), using the PCM solvation model PCM for acetonitrile. The calculations obtained did not yield any imaginary frequencies. Later, the excitation energies carried out trough TD-DFT calculations. Lastly, the excitation energies were corrected by means of calculations of the state-specific solvation of the vertical excitation. For the TD-DFT and TD-DFT calculations with state-specific correction, the same functionals, base set and solvation model were used. The input files shown below, correspond to the ground state equilibrium geometry optimization. The Z-matrix coordinates of the optimized geometries for SAP and IR-780 are included in a different section below.

Gaussian input file example for the SAP molecule ground state equilibrium geometry optimization.

```
%nprocshared=16
%mem=32gb
%chk=SAP.chk
#p pbe1pbe/6-311++g(d,p) opt=calcfc freq scrf=(pcm,solvent=acetonitrile) nosymm int=grid=ultrafine iop(1/8=3) scf=xqc
density=current

SAP_S0_acetonitrile

0 1
[Z-matrix coordinates of the input structure]
```

Gaussian input file for the SAP molecule to the vertical excitations calculation.

```
%nprocshared=16
%mem=32gb
%oldchk=SAP.chk
%chk=TDSAP.chk
#p pbe1pbe/6-311++g(d,p) TD=(NStates=20,singlets,root=2) scrf=(pcm,solvent=acetonitrile) nosymm int=grid=ultrafine
iop(1/8=3) scf=xqc density=current geom=check guess=read

SAP_TD_acetonitrile

0 1
[No coordinates in Z-matrix because chosen the SAP.chk file to start the TD-DFT calculation using geom=check and
guess=read as keywords]
```

Gaussian input file for the SAP molecule to TD-DFT state-specific solvation of the vertical excitation calculation.

```
%nprocshared=16
%mem=32gb
%oldchk=SAP.chk
%chk=SAPSS.chk
#p pbe1pbe/6-311++g(d,p) scrf=(pcm,solvent=acetonitrile,read) nosymm int=grid=ultrafine iop(1/8=3) scf=xqc
density=current geom=check guess=read

SAP_state_specific_acetonitrile_01

0 1

NonEq=Write

--Link1--
%nprocshared=16
%mem=32gb
%chk=SAPSS.chk
#p pbe1pbe/6-311++g(d,p) scrf=(pcm,solvent=acetonitrile,ExternalIteration,Read) TD=(NStates=20,singlets,root=1) nosymm
int=grid=ultrafine iop(1/8=3) scf=xqc density=current geom=check guess=read

SAP_state_specific_acetonitrile_02

0 1
NonEq=read
```

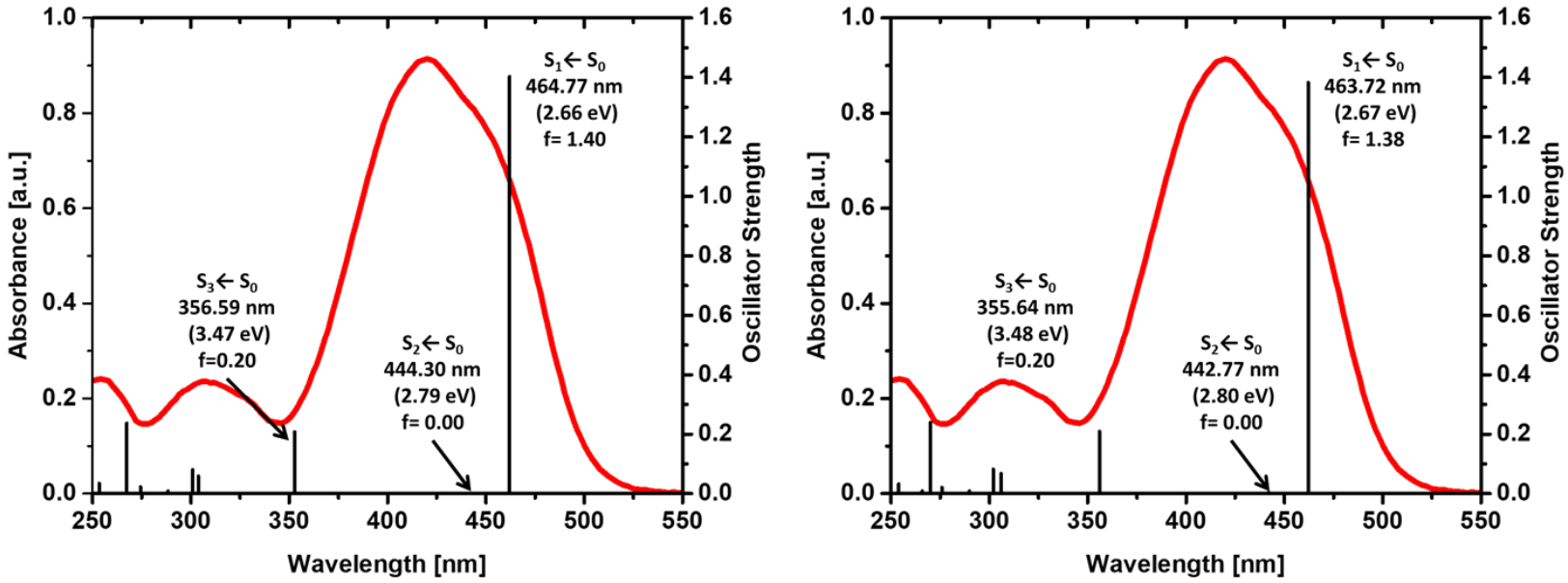

Figure S8. SAP Experimental absorption spectra (red line) comparison with the calculated vertical transitions (black lines) calculated using TD-DFT PBE0/6-311++G(d,p) (left) and M06/6-311G++(d,p) (right)with PCM as MeCN solvent model.

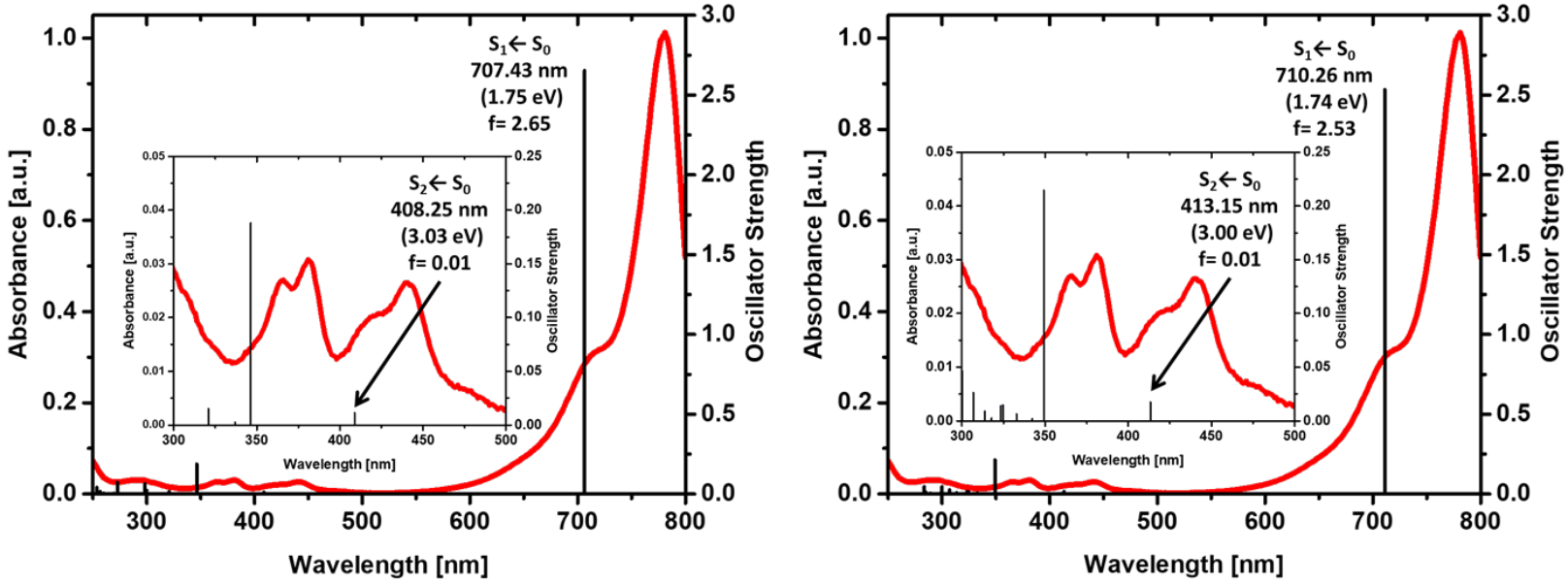

Figure S9. IR780 experimental absorption spectra (red lines) and comparison with the calculated vertical transitions (black lines) using TD-DFT PBE0/6-311++G(d,p) (left) and M06/6-311++G(d,p) (right) with PCM as the solvent model for acetonitrile. An expanded view of the spectra from 200 to 500 nm is included in the insets.

Energy Transfer Rate Constant Calculation (Förster model)

The rate of transfer k_{trans} can be calculated using the equation S1 which considera a coulombic type interaction for the interchromophore coupling.

$$k_{trans} = \frac{9000 \ln(10) \kappa^2 \Phi_{f(D)} J}{128 \pi^5 N n^4 \tau R^6} \quad \text{(S1)}$$

Where is κ^2 the orientation factor of the donor and acceptor transition dipole moments, $\Phi_{f(D)}$, is the donor fluorescence quantum yield in the absence of any acceptor, J, is the spectral overlap, N is Avogadro's number, n, is the solvent's refractive index, τ, is the donor fluorescence lifetime and R is the donor–acceptor center-to-center distance of separation. The spectral overlap is:

$$J = \int_0^\infty \frac{f_s(\nu)\varepsilon_A(\nu)}{\nu^4} d\nu \quad \text{(S2)}$$

where $f_s(\nu)$ is the normalized spectral distribution of fluorescence intensity as a function of wavenumber, $\varepsilon_A(\nu)$, is the molar absorption coefficient of the acceptor as a function of wavenumber.

The Foster distance R_0 which is a critical distance between the center of donor and acceptor where the transfer efficiency is 50% value is:

$$R_0^6 = \frac{9000 \ln(10) \kappa^2 \Phi_{f(D)} J}{128 \pi^5 N n^4} \quad \text{(S3)}$$

The Transfer efficiency, T, can be calculated using Equation S4.

$$T = \frac{R_0^6}{R^6 + R_0^6} \quad \text{(S4)}$$

The calculation of the Föster energy transfer parameters was performed using the program PhotochemCAD™.[17]

In the following pages we include three different ways to calculate the Förster efficiency. In all cases we use the S_2 emission spectrum of IR-780 but change the way we consider the acceptor chromophore absorption transitions. We include the calculations using the SAP absorption spectrum (Figure S11), the Cy-SAP absorption spectrum (Figure S12), and the Cy-SAP minus IR-780 absorption spectrum (Figure S13, also see Figure S10). All these different ways to estimate the overlap integral give similar results, with efficiencies from 75 to 81%. The manuscript refers to the calculation according to the overlap displayed in Figure S11 which considers the SAP absorption spectrum.

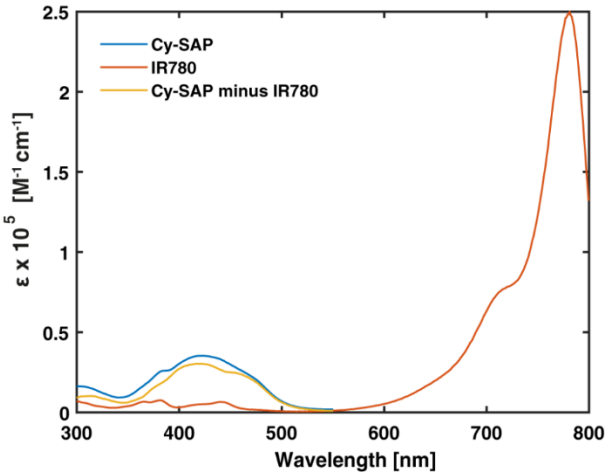

Figure S10. Comparison between the Cy -SAP and the IR780 absorption spectra. We also include the spectrum that results from the substraction of the Cy-SAP spectrum minus IR780 absorption spectra. This spectrum is nearly identical to that of SAP. This comparison was made in order to show that the two chromophores maintain their spectroscopic properties in Cy-SAP.

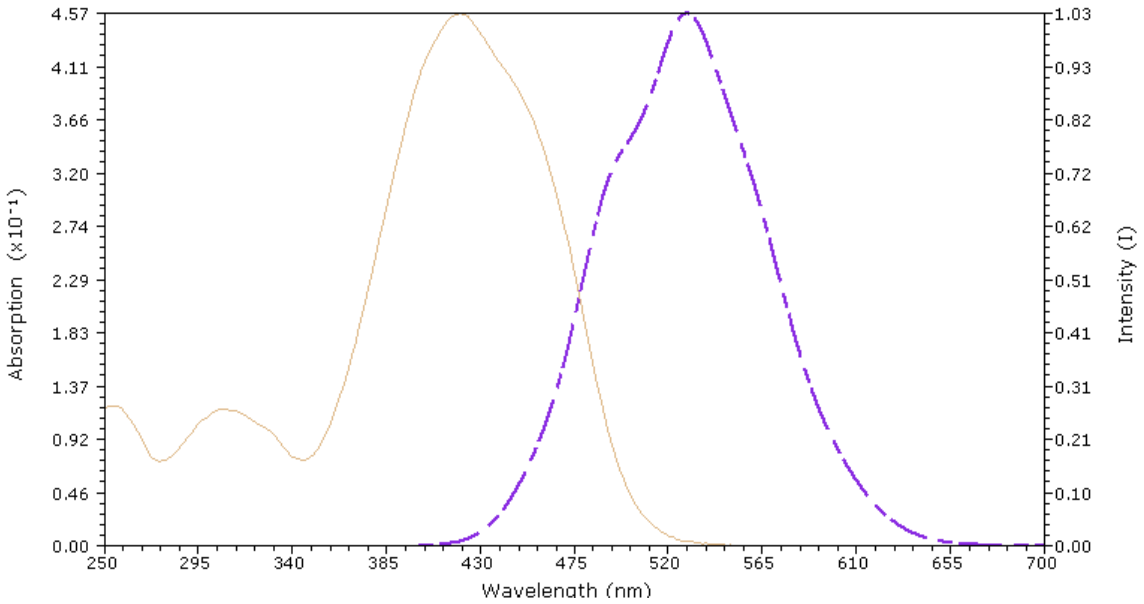

Figure S11. Overlap between absorption spectrum of SAP (orange line) and emission spectrum of the S_2 state of IR780 (purple line). The latter spectrum was formed with two log-normal functions which were fitted to the experimental data as indicated in a previous figure.

Table S1. Results of the Förster energy transfer calculations in Cy-SAP using the orientation factors obtained with TD-DFT calculations, and the overlap in Figure S11. The interchromophore distance was 0.925 nm which corresponds to the center-to-center distance of the two chromophores from the respective optimized geometry. For reference we include the results from considering random relative orientations between the chromophores ($\kappa^2 = 2/3$).

	$\kappa^2 = 2/3$	PBE0 ($\kappa^2 = 3.76$)	M06 ($\kappa^2 = 3.73$)
J [cm^6mmol^{-1}]	$2.3x10^{-14}$	$2.3x10^{-14}$	$2.3x10^{-14}$
Förster distance [Å]	8.3	11.1	11.1
Transfer efficiency [%]	34.7	75.0	74.8
k_{trans} [s^{-1}]	$3.8x10^{11}$	$2.1x10^{12}$	$2.1x10^{12}$
Dexter value [eV^{-1}]	0.116	0.116	0.116

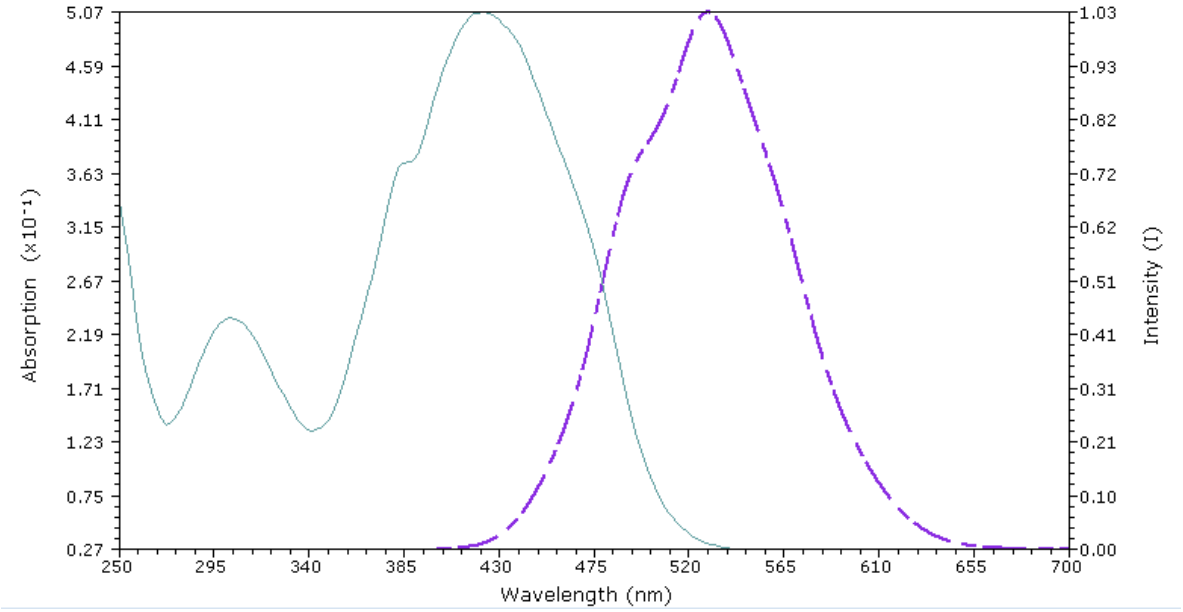

Figure S12. Overlap between absorption spectrum of Cy-SAP (blue line) and emission spectrum of S_2 excited state of the IR780 (purple line).

Table S2. Results of Förster energy transfer calculations in Cy-SAP using orientation factors obtained with TD-DFT theory and the overlap in Figure S12. For reference we include the results from considering random relative orientations between the chromophores (κ^2 = **2/3**).

	κ^2 = (2/3)	PBE0 (κ^2= 3.76)	M06 (κ^2= 3.73)
J [cm^{6}mmol^{-1}]	3.1x10^{-14}	3.1x10^{-14}	3.1x10^{-14}
Förster distance [Å]	8.8	11.8	11.7
Transfer efficiency [%]	41.6	80.1	80.0
k_{trans} [s^{-1}]	5.1x10^{11}	2.9x10^{12}	2.9x10^{12}
Dexter value [eV^{-1}]	0.123	0.123	0.123

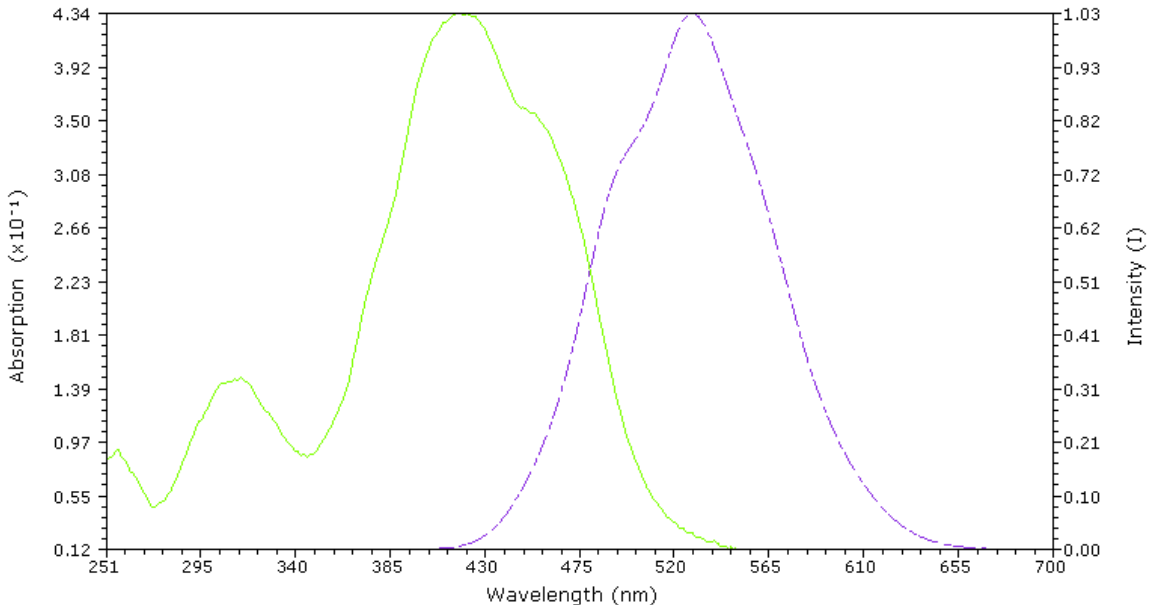

Figure S13. Overlap between absorption spectrum of Cy-SAP minus IR780 (green line) and emission spectrum of the S_2 excited state of the IR780 (purple line).

Table S3. Results of Förster energy transfer calculation in Cy-SAP using orientation factors obtained with TD-DFT theory and the overlap in Figure S13. For reference we include the results from considering random relative orientations between the chromophores (κ^2 = **2/3**).

	κ^2 = (2/3)	PBE0 (κ^2 = 3.76)	M06 (κ^2 = 3.73)
J [cm^6mmol^{-1}]	$3.1x10^{-14}$	$3.1x10^{-14}$	$3.1x10^{-14}$
Förster distance [Å]	8.8	11.7	11.7
Transfer efficiency [%]	41.7	80.1	80.0
k_{trans} [s^{-1}]	$5.1x10^{11}$	$2.9x10^{12}$	$2.9x10^{12}$
Dexter value [eV^{-1}]	0.156	0.156	0.156

***E-Z* Photo-transformation of the Actuator (SAP alone)**

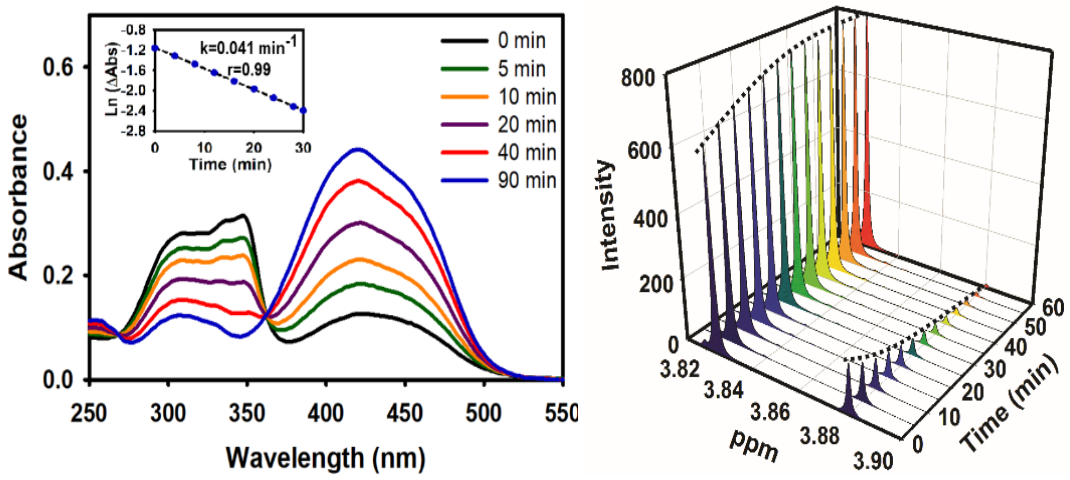

Figure S14. Evidence of the phototransformation of the SAP system and the return to the thermally stable isomer (E). On the left we show the spectral evolution associated with the Z-E thermal back-transformation. On the right we include the proton NMR spectrum as a function of time for the Z-E thermal back-transformation. The signal at 3.88 ppm corresponds to the *N*-methyl proton of the Z isomer and the signal at 3.825 pm, to the same proton in the E-isomer.

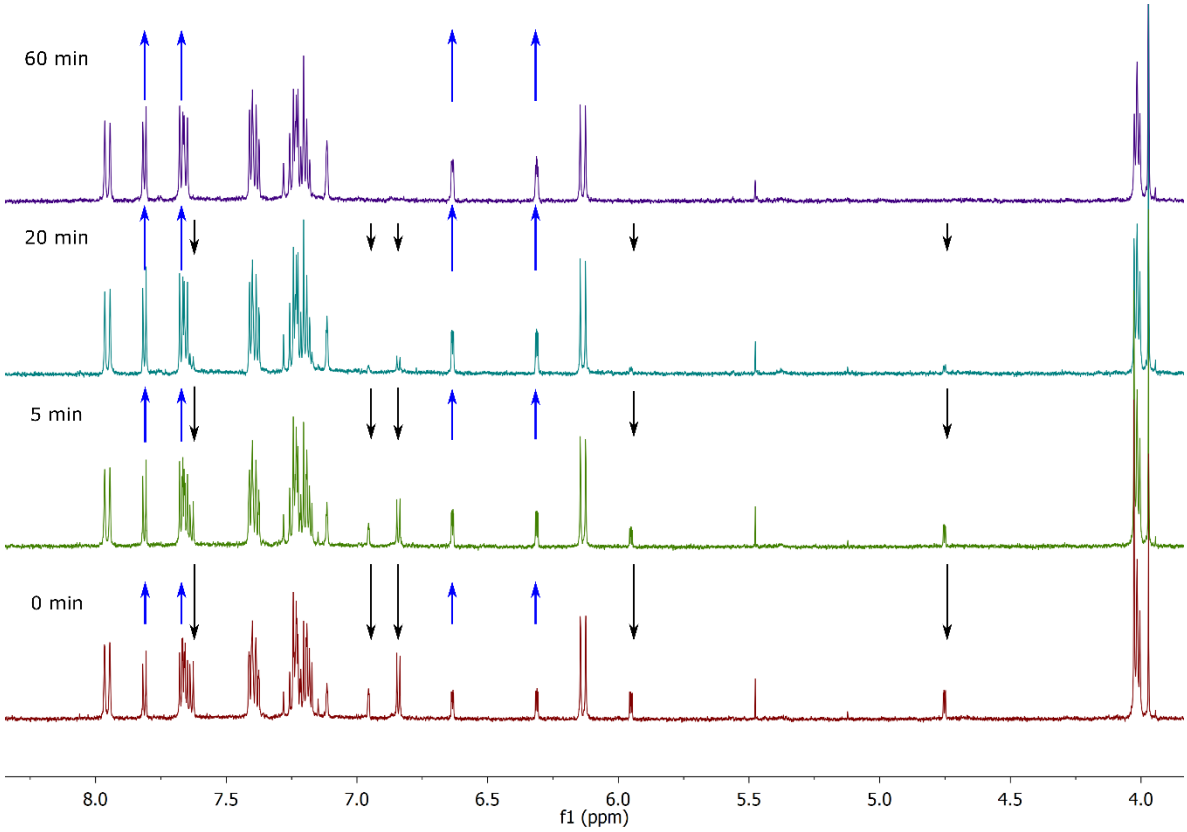

Figure S15. **^{1}H** Spectral evolution of the Z→E thermal back-isomerization of Cy-SAP. The complete disappearance of the Z isomer is more clearly observed in the full spectra. Important signals are marked with arrows next to the signals.

Estimation of the absorption spectra of the E-SAP and E-Cy-SAP isomers from the photostationary spectra

The method used to obtain an estimation of the absorption spectra for each isomer is based on the one proposed by Calbo and coworkers.[18] Starting from the Lambert-Beer law for the photostationary state:

$$\boldsymbol{A_{PSS}(\lambda) = l\left(\varepsilon_E(\lambda)C_E(PSS) + \varepsilon_Z(\lambda)C_Z(PSS)\right)} \quad \text{(S5)}$$

Where $\boldsymbol{A_{PSS}(\lambda)}$ is the total absorbance in the photostationary state as a function of the wavelength, $\boldsymbol{l}$ is the path length (in cm^{-1}), $\boldsymbol{\varepsilon_E(\lambda)}$ and $\boldsymbol{\varepsilon_Z(\lambda)}$ (in L mol^{-1} cm^{-1}) are the molar extinction coefficients as a function of wavelength of the *trans*- and *cis*- isomers respectively.

Rearranging for $\boldsymbol{\varepsilon_E(t)}$ from Equation S5:

$$\boldsymbol{\varepsilon_Z(\lambda) = \frac{\frac{A_{PSS}(\lambda)}{l} - \varepsilon_E(\lambda)C_E(PSS)}{C_Z(PSS)}} \quad \text{(S6)}$$

It is known that the total concentration $\boldsymbol{C_0}$ remains constant throughout the isomerization process and is also the sum of the concentration of both isomers.

$$\boldsymbol{C_0 = C_E(PSS) + C_Z(PSS)} \quad \text{(S7)}$$

The concentration of trans- and cis- isomers in the photostationary state was estimated using a specific wavelength where the trans isomer is the main absorbent.

$$\boldsymbol{C_E(PSS) = f\left(\frac{A_{PSS}(\lambda_{specific})}{\varepsilon_E(\lambda_{specific})}\right)} \quad \text{(S8)}$$

$$\boldsymbol{C_Z(PSS) = \frac{A_{t=0}(\lambda_{specific})}{\varepsilon_E(\lambda_{specific})} - C_E(PSS)} \quad \text{(S9)}$$

where $\boldsymbol{A(\lambda_{specific})}$ is the absorbance before irradiation in a specific wavelength where the absorbance of the *cis*- isomer is minimal, $\boldsymbol{A_{PSS}(\lambda_{specific})}$ is the absorbance after irradiation in the photostationary state at the same wavelength and $\boldsymbol{f}$ is a relation between the *trans*- and *cis*- isomer's absorbance at the $\boldsymbol{\lambda_{specific}}$.

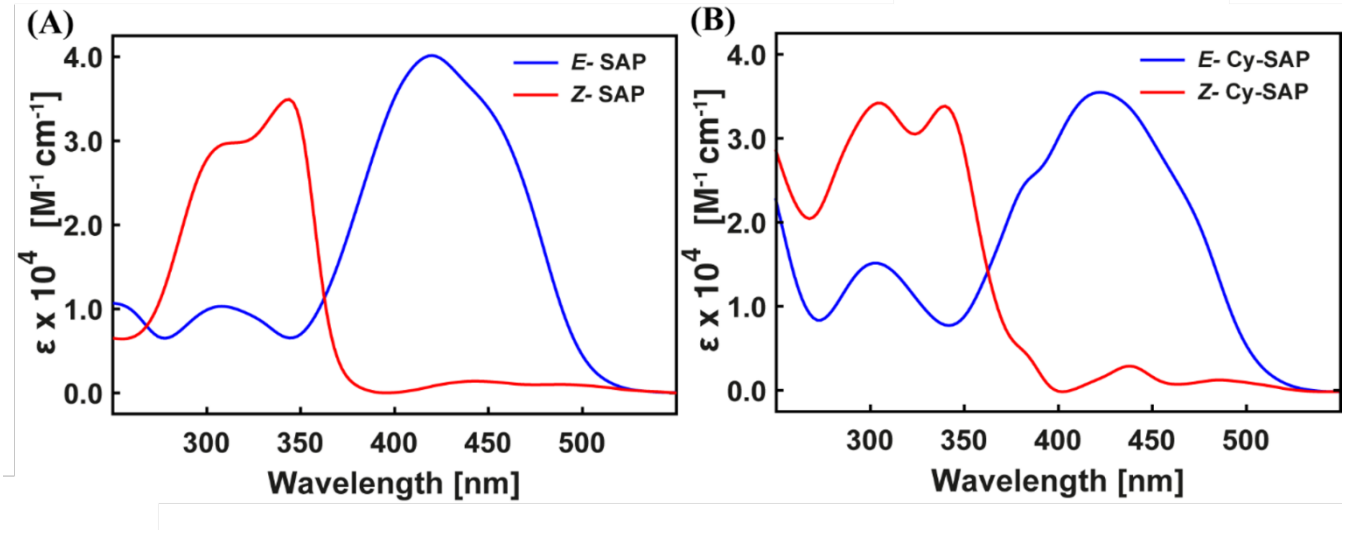

Figure S16. (A) Absorption spectrum of (E) SAP and (Z) SAP. (B) Absorption spectrum of (E) Cy-SAP and of (Z) Cy-SAP

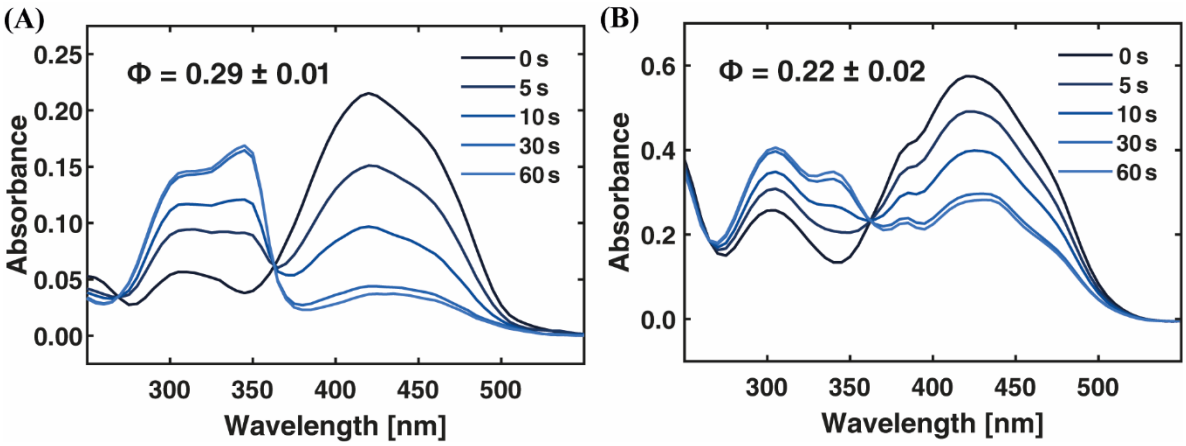

Figure S17. Spectra showing the data used to calculate the photoisomerization quantum yield for monophotonic excitation in the formation of the photostationary state of SAP (A) and Cy-SAP (B) irradiating with 405 nm 3 mW laser. The thermal back isomerization is also included for both systems.

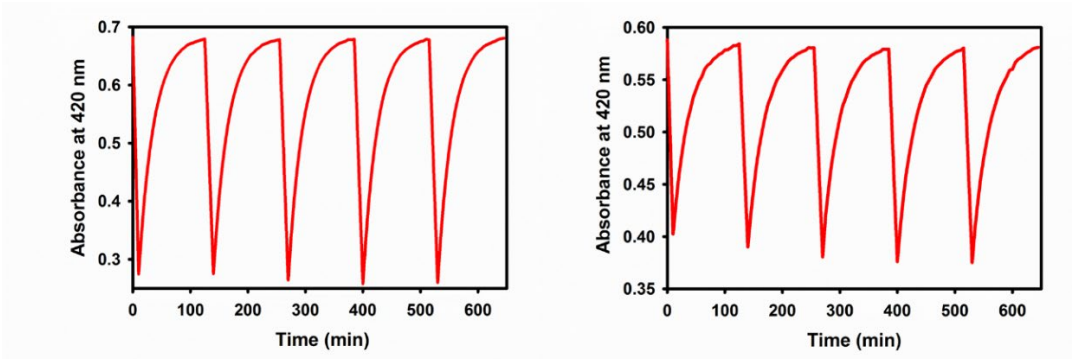

Figure S18. Photoisomerization-cycles of SAP system (left) and Cy-SAP system (right). Both experiments were made in acetonitrile

Non-linear NIR light Excitation and Photoisomerization of Cy-SAP

Non-linear photocontrol of the Cy-SAP system through energy transfer from the cyaninic antenna to the azo linkage effector was demonstrated with the following experiment. Cy-SAP was used after recrystalization from DCM/ether. Acetonitrile (HPLC) was used for the measurements. The solutions were used immediately after preparation. The experimental setup is shown in Scheme S1.

The same laser system as the fluorescence up-conversion experiments was used. The laser system produces pulses of 100-200 fs, 860 nm at 1kHz repetition rate. The output beam power was adjusted trough a neutral density filter (NDF) and focused with a lens (Thorlabs, f=1000 mm) into a 0.5 cm quartz cell containing 400 mL of the solutions (stirring, in darkness and sealed). The isomerization from the azo moiety is monitored by taking UV-Vis spectra prior and after NIR irradiation.

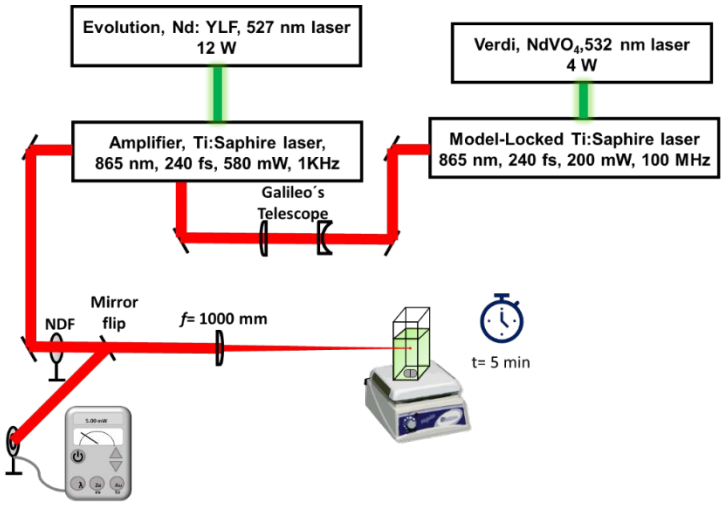

Scheme S1. Experimental setup for non-linear photoisomerization of Cy-SAP.

In order to determine the intensity levels where no Cy-SAP photodegradation is observed from multiphoton ionization and other irreversible multiphoton events, the samples were irradiated for 5 minutes at 3-20 mW average powers ($2x10^{10}$-$2x10^{11}$ W cm^{-2} peak irradiance) with the pulsed NIR source tuned to 860 nm. The spectra in Figure S19 show there is no change at wavelengths above 600 nm when exciting the sample at powers up to 10 mW, indicating no cyanine decomposition. When working in these powers, the only change observed is the one due to the isomerization of the azo linkage as observed in the 250—500 nm region. Evidence of photodecomposition is observed only when irradiating at average powers larger than or equal to 20 mW. At average powers larger than this, the cyaninic absorption above 600 nm drops by a small percentage, suggesting some decomposition of the antenna due to the large irradiation intensity. Furthermore, at these larger intensities, the isomerization around the azo moiety is not observed given there is no change in absorption around 420 nm, further indicating non-linear optical decomposition at these higher intensities, most likely due to multiphoton ionization.

Although a small yield dissociation of the ether linked group has been observed in a related system previously by our group upon non-linear excitation (a different system, designed for such purposes),[19] no evidence of this was seen for the Cy-SAP system. For the system of ref. 17, the meso-attached group was specifically designed for homolytic dissociation, which is achieved in a small yield of $2x10^{-3}$ per excitation event (which is appropriate for the application of that system). In fact, in ref. 17 we included an example of a different attached meso substituent which does not undergo dissociation, which shows that meso-group photodissociation is not a general feature in this kind of molecule.

Further evidence that the Cy-SAP molecule does not undergo photo-destruction at the $2x10^{10}$-$2x10^{11}$ W cm^{-2} intensity levels comes from the observation that when the sample is allowed to rest at room temperature after irradiation, there is a full recovery to the initial state after with a clear isosbestic point at 365 nm (Figure S25). Moreover, if the dissociation was to occur, the band at 425 nm would show changes in shape, absorbance and position. It should be noticed that the first band of the stilbenylazopyrrole unit in the phenol form has a more square-like form with a larger absorption coefficient. The differences in these bands between SAP and Cy-SAP is highlighted in Figure S26.

The quadratic dependence of the azo-linkage isomerization as a function of irradiation power was tested using the same setup in a power range where no degradation is observed (2-7 mW or $2\text{-}5x10^{10}$ W cm^{-2} peak irradiance).

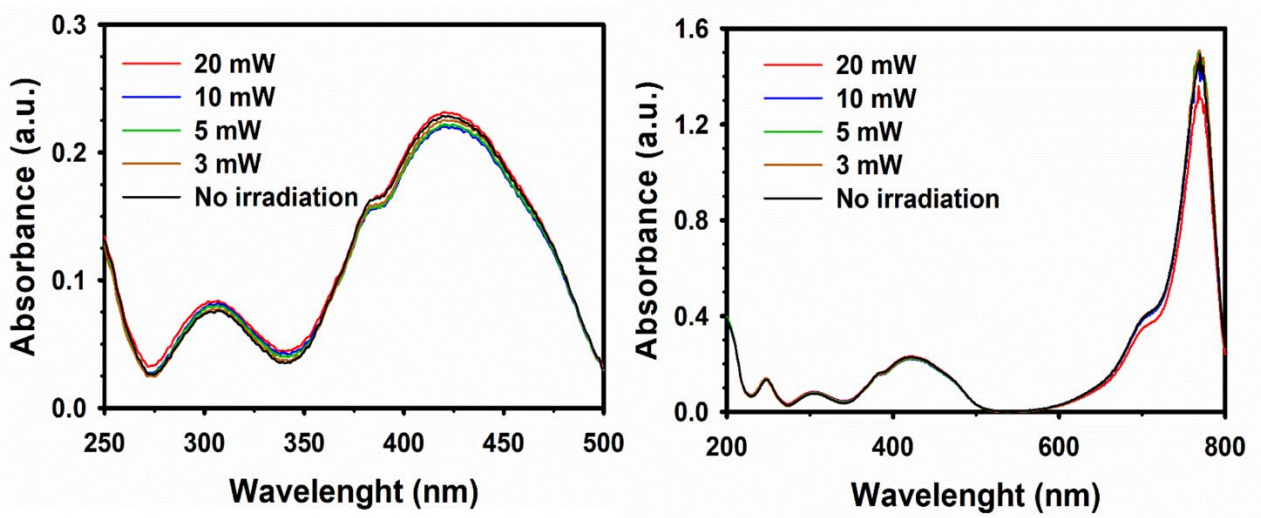

Figure S19. Photodecomposition intensity threshold. The spectra where taken after NIR irradiation and compared to the spectrum prior to irradiation. Right: The full spectral window shows no decomposition at intensities up to 10 mW. Left: Close up of the 250-500 nm spectral region, different behavior is seen at 20 mW irradiation power.

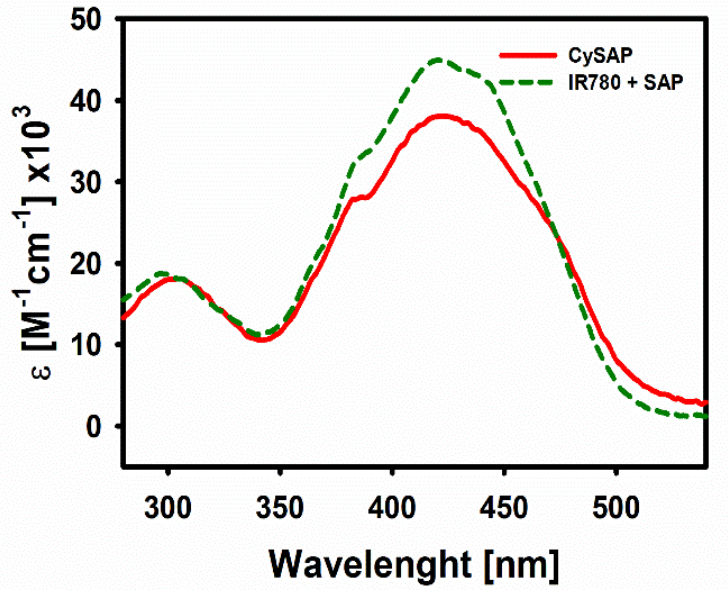

Figure S20. Absorption spectrum of Cy-SAP (red line) and for comparison, the sum of the absorption spectra of SAP and IR780 focusing in the 300-500 nm spectral range.

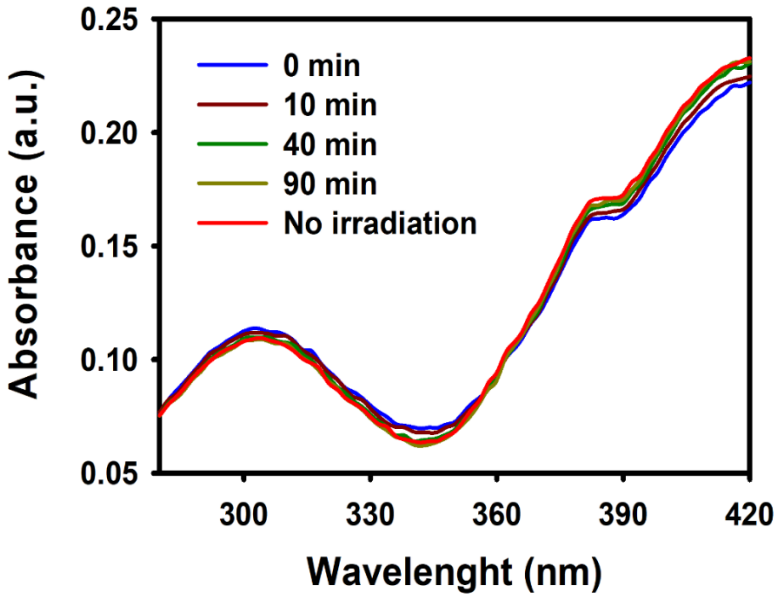

Figure S21. Cy-SAP thermal back-isomerization (Z→E) after two-photon excitation at 860 nm. A clear isosbestic point is seen at 370 nm. Full relaxation to the original spectrum is seen. The two-photon induced reaction takes place in the center of a 3 ml sample cell so that the spectra can be acquired in a UV-Vis spectrophotometer. It should be noticed that the transformation occurs in a small volume of the order of a few cubic microns, but the spectra are representative of the mixed 3 ml sample, therefore, the net transformation in the full cell´s volume is small despite the fact that the phenomena occurs in a localized fashion in the center of the sample (where the local concentration for the E-Z isomerization by two photon absorption can be much higher).

Time-resolved Fluorescence Spectroscopy

Table S4. Parameters for the Fluorescence Decay of the S_2 state of IR780 in Ethanol Solutions.

λ_{fluo} [nm]	τ_1 [fs][ps]	τ_1 [%]	τ_2 [ps]	α_2 [%]
480	0.18±0.1	88.2	1.45±0.2	11.8
500	0.21±0.1	83.3	1.45±0.2	16.7
520	0.26±0.1	74.0	1.45±0.2	26.0
530	0.23±0.1	72.1	1.45±0.2	27.9
540	0.22±0.1	63.0	1.45±0.2	37.0
560	0.21±0.1	68.7	1.45±0.2	31.3

λ_{exc} = 860 nm. IRF ~200 fs.

Table S5. Parameters for the Fluorescence Decay of the S_2 state of SAP and Cy-SAP in Acetonitrile Solution.

λ_{fluo} [nm]	τ_{SAP} [fs]	$\tau_{Cy\text{-}SAP}$ [fs]
475	200 ± 100	170 ± 20
500	240 ± 60	200 ± 20
525	260 ± 30	170 ± 20
550	260 ± 10	180 ± 10
575	300 ± 20	190 ± 10
600	300 ± 20	180 ± 20
625	-----	200 ± 10

λ_{exc} = 860 nm. IRF ~300 fs.

Anisotropy and Fluorescence Up-Conversion Experiments

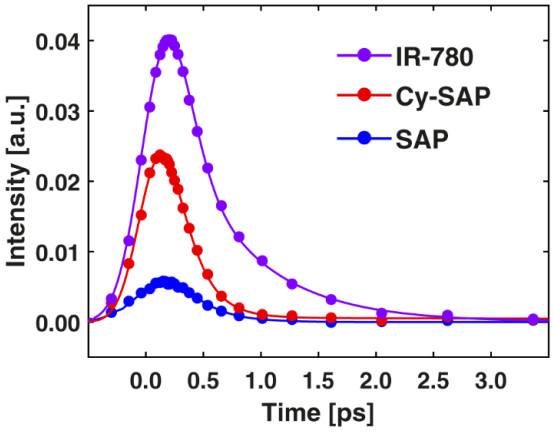

Figure S22. Comparison of absolute fluorescence intensities between SAP IR-780 Cy-SAP. The detection and excitation wavelengths were 500 nm and 860 nm (two photon) respectively. The IR-780 were taken in a back-to-back fashion. The up-conversion experiments for SAP required an increase in the solution concentration and a two-fold increase in the pulse energy due to its reduced two-photon absorption cross section.

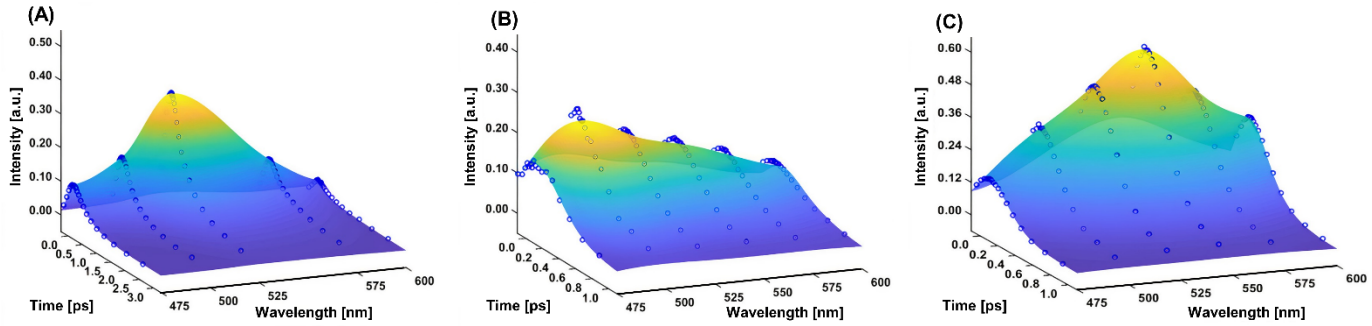

Figure S23. Time resolved emission spectra from (A) IR-780 and (B) SAP and (C) Cy-SAP. The emission is produced by two-photon 860 nm excitation. The solvent in all cases was methanol. The symbols indicate the experimental up-conversion signals and the coloured surfaces were interpolated from these data.

inetic Scheme for the Antenna-Actuator system (Cy-SAP):

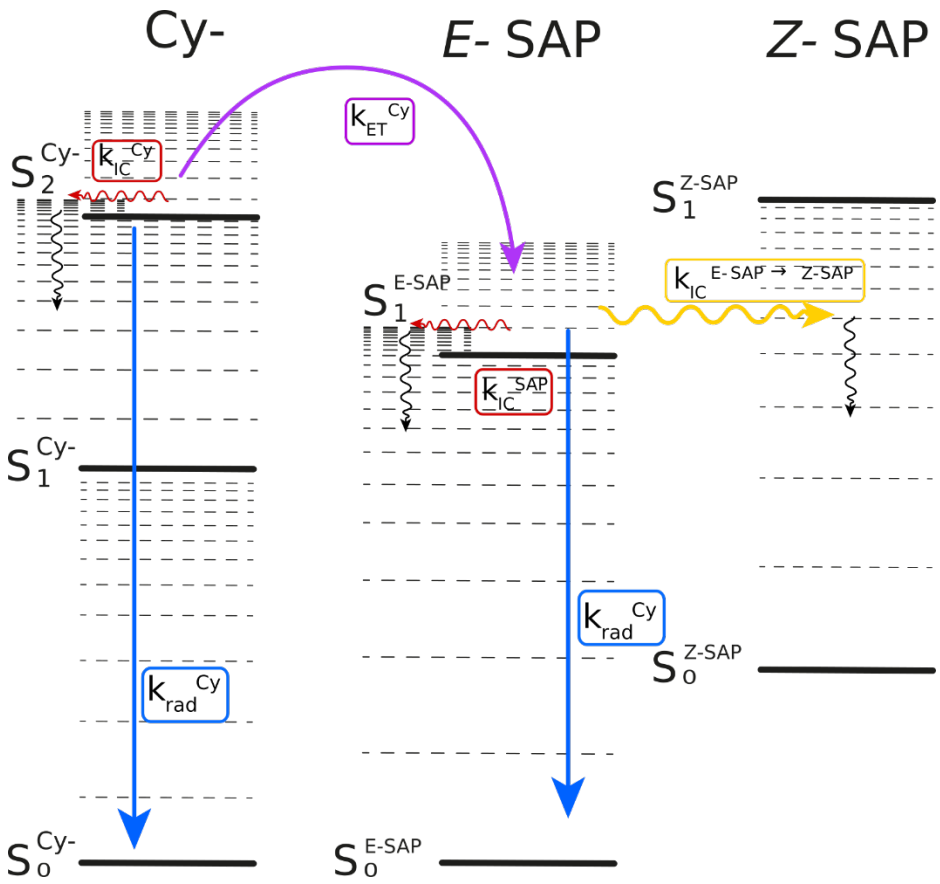

Scheme S2. Kinetic scheme of the system Antenna-Actuator (Cy-SAP).

Starting with the population of the second singlet excited state located at the cyanine section (S_2^{Cy}) by two-photon absorption, the system can evolve through energy transfer to form the first singlet excited state of the actuator section: **(E) SAP** (S_1^{E-SAP}). This population can then undergo isomerization to form the **Z** isomer after internal conversion to the ground state potential energy surface. The energy transfer channel exists in kinetic competition with internal conversion within the states localized in the cyanine section. The radiative channels are quite minor but can be used to follow the population of the excited states.

For S_2^{Cy} the elemental processes are:

$$S_2^{Cy} \xrightarrow{\kappa_{rad}^{Cy}} S_0^{Cy} + h\nu^{Cy} \quad \text{(S10)}$$

$$S_2^{Cy} \xrightarrow{\kappa_{IC}^{Cy}} S_1^{Cy} \quad \text{(S11)}$$

$$S_2^{Cy} \xrightarrow{\kappa_{ET}^{Cy}} S_1^{E-SAP} \quad \text{(S12)}$$

Where (S10) corresponds to the radiative decay, (S11) to internal conversion to the first cyanine-localized excited state, and (S12) to the energy transfer channel.

For S_1^{E-SAP} the processes are:

$$S_1^{E-SAP} \xrightarrow{\kappa_{rad}^{E-SAP}} S_0^{E-SAP} + h\nu^{E-SAP} \quad \text{(S13)}$$

$$S_1^{E-SAP} \xrightarrow{\kappa_{IC}^{E-SAP}} S_0^{E-SAP} \quad \text{(S14)}$$

$$S_1^{E-SAP} \xrightarrow{\kappa_{IC}^{E-SAP \to Z-SAP}} S_0^{E-SAP} \quad \text{(S15)}$$

Where the channel in (S13) is the emission decay from S_1^{E-SAP} (radiative channels are of course small in yield but were used to monitor the kinetics). The channels in (S14) and (S15) correspond to the return to the electronic ground state leading to each isomer respectively.

We can write the kinetic equations for the concentration of S_2^{Cy} as a function of time $[S_2^{Cy}(t)]$ and the concentration of S_1^{E-SAP} as a function of time $[S_1^{E-SAP}(t)]$, which are the two bright states of the system at the detection wavelengths.

$$-\frac{d}{dt}[S_2^{Cy}(t)] = [S_2^{Cy}(t)](\kappa_{rad}^{Cy} + \kappa_{IC}^{Cy} + \kappa_{ET}^{Cy}) \quad \text{(S16)}$$

$$-\frac{d}{dt}[S_1^{E-SAP}(t)] = [S_1^{E-SAP}(t)](\kappa_{rad}^{E-SAP} + \kappa_{IC}^{E-SAP} + \kappa_{IC}^{E-SAP \to Z-SAP}) - [S_2^{Cy}(t)](\kappa_{ET}^{Cy}) \quad \text{(S17)}$$

The last term in equation (S17) corresponds to the formation channel of S_1^{E-SAP} through energy transfer. Identifying κ_{Total}^{Cy} as the sum of the Cy-localized S_2 decay constants and κ_{Total}^{E-SAP} as the sum of SAP (E) S_1 decay constants, equations (S16) and (S17) are:

$$-\frac{d}{dt}[S_2^{Cy}(t)] = [S_2^{Cy}(t)]\,\kappa_{Total}^{Cy} \quad \text{(S18)}$$

$$-\frac{d}{dt}[S_1^{E-SAP}(t)] = [S_1^{E-SAP}(t)]\,\kappa_{Total}^{E-SAP} - [S_2^{Cy}(t)]\,\kappa_{ET}^{Cy} \quad \text{(S19)}$$

Equation (S18) corresponds to a fist-order reaction, with solution:

$$[S_2^{Cy}(t)] = [S_2^{Cy}(0)]e^{-(\kappa_{Total}^{Cy})t} \quad \text{(S20)}$$

Substituting the previous equation, in the differential equation of S_1^{E-SAP} (equation S19).

$$-\frac{d}{dt}[S_1^{E-SAP}(t)] = [S_1^{E-SAP}(t)]\,\kappa_{Total}^{E-SAP} - \kappa_{ET}^{Cy}[S_2^{Cy}(0)]e^{-(\kappa_{Total}^{Cy})t} \quad \text{(S21)}$$

Gives the following solution where $[S_1^{E-SAP}(t=0)] = 0$.

$$[S_1^{E-SAP}(t)] = \frac{\kappa_{ET}^{Cy}}{\kappa_{Total}^{E-SAP} - \kappa_{Total}^{Cy}}[S_2^{Cy}(0)]\left(e^{-(\kappa_{Total}^{Cy})t} - e^{-(\kappa_{Total}^{E-SAP})t}\right) \quad \text{(S22)}$$

Defining:

$$\kappa^{E-SAP} = \frac{\kappa_{ET}^{Cy}}{\kappa_{Total}^{E-SAP} - \kappa_{Total}^{Cy}} \quad \text{(S23)}$$

Equation (S22) can be written as follows.

$$[S_1^{E-SAP}(t)] = \kappa^{E-SAP}[S_2^{Cy}(0)]\left(e^{-(\kappa_{Total}^{Cy})t} - e^{-(\kappa_{Total}^{E-SAP})t}\right) \quad \text{(S24)}$$

From the up-conversion experiments, the total decay rate constants for Cy S_2 and SAP S_1 are $(\kappa_{Total}^{Cy} \simeq 6\,\mathrm{x}\,10^{12}\,[s^{-1}])$, $(\kappa_{Total}^{E-SAP} \simeq 4\,\mathrm{x}\,10^{12}[s^{-1}])$. From the simple Förster model, the rate constant for energy transfer was estimated above to be approximately $(\kappa_{ET}^{Cy} \simeq 3\,\mathrm{x}\,10^{12}\,[s^{-1}])$.

With these considerations $[S_2^{Cy}(t)]$ and $[S_1^{E-SAP}(t)]$ evolve as follows:

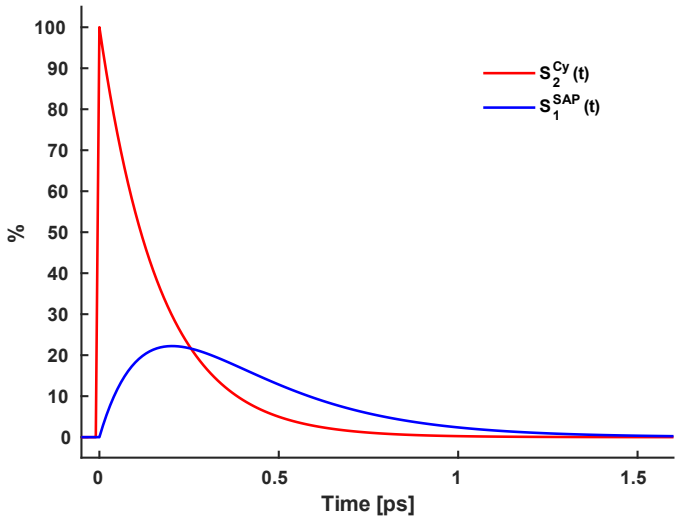

Figure S24. Concentration [%] as a function of time for both emissive states S_2^{Cy} (red) and S_1^{E-SAP} (blue).

Fluorescence signals

The fluorescence signal as a function of time is proportional to the number of photons being emitted per unit time from the sample by both states since both emit in the region where the fluorescence was detected (475 to 600 nm, see the manuscript): $\boldsymbol{hv^{Cy}(t)}$ and $\boldsymbol{hv^{E-SAP}(t)}$.

The kinetic equations of these processes are:

$$\frac{\boldsymbol{d}}{\boldsymbol{dt}}[\boldsymbol{hv^{Cy}(t)}] = \left[\boldsymbol{S_2^{Cy}\,(t)}\right]\boldsymbol{\kappa_{rad}^{Cy}} \tag{S25}$$

$$\frac{\boldsymbol{d}}{\boldsymbol{dt}}[\boldsymbol{hv^{E-SAP}(t)}] = [\boldsymbol{S_1^{E-SAP}\,(t)}]\,\boldsymbol{\kappa_{rad}^{E-SAP}} \tag{S26}$$

The total fluorescence intensity is the sum of the fluorescence intensity of both states $S_2^{Cy}\,(t)$ and $S_2^{E-SAP}\,(t)$, therefore the total intensity as a function of time is:

$$\boldsymbol{I_{fluo}(t)} \simeq \boldsymbol{\kappa_{rad}^{Cy}}\; \boldsymbol{e^{-\left(\kappa_{Total}^{Cy}\right)t}} + \boldsymbol{\kappa_{rad}^{E-SAP}\kappa^{E-SAP}}\left(\boldsymbol{e^{-\left(\kappa_{Total}^{Cy}\right)t}} - \boldsymbol{e^{-\left(\kappa_{Total}^{E-SAP}\right)t}}\right) \tag{S27}$$

We can rewrite the previous equation in order to obtain an expression in terms of ratio between the radiative constants (this relation may vary slightly across the spectrum due to the different vibro-electronic transitions of each state).

$$\boldsymbol{I_{fluo}(t)} \simeq \left(\frac{\boldsymbol{\kappa_{rad}^{Cy}}}{\boldsymbol{\kappa_{rad}^{E-SAP}}}\right)\boldsymbol{e^{-\left(\kappa_{Total}^{Cy}\right)t}} + \boldsymbol{\kappa_{rad}}\left(\boldsymbol{e^{-\left(\kappa_{Total}^{Cy}\right)t}} - \boldsymbol{e^{-\left(\kappa_{Total}^{E-SAP}\right)t}}\right) \tag{S28}$$

The fluorescence detected at 500 nm is a convolution between the fluoresce signal $\boldsymbol{I_{fluo}}$ with the instrumental response function $\mathrm{I_{IRF}}$ of our up-conversion setup which is a gaussian function with a FWHM of 270 fs.

$$\boldsymbol{I_{fluo}^{Convolution}(t)} = \int_{t'} \mathbf{I_{IRF}(t - t')}\,\boldsymbol{I_{fluo}(t')} \tag{S29}$$

From the absorption spectrum, the relation between the radiative constants for the second excited state localized in the cyaninic section $\boldsymbol{\kappa_{rad}^{Cy}}$ and the first excited state localized in the azo section $\boldsymbol{\kappa_{rad}^{E-SAP}}$ is $\left(\frac{\boldsymbol{\kappa_{rad}^{Cy}}}{\boldsymbol{\kappa_{rad}^{E-SAP}}} \simeq \frac{\mathbf{1}}{\mathbf{4}}\right)$. This value was estimated using the relation between the molar extinction coefficients in the region of 450 nm (see Figure S10).

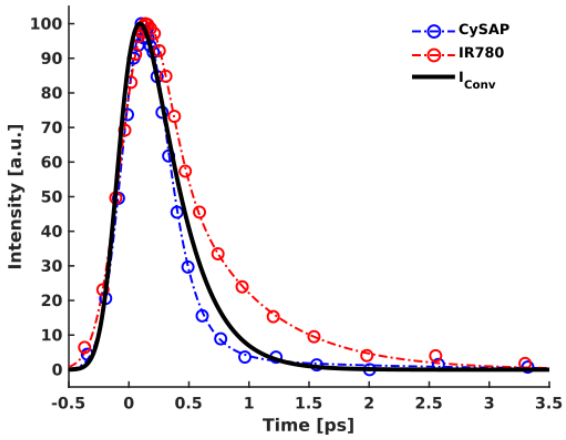

Figure S25. Fluorescence up-conversion traces of Cy-SAP (blue symbols) and IR780 (red symbols).

The black thick line is the result of the kinetic model that simulates the total convoluted fluorescence intensity [a.u.] as a function of time. The emission is considered to come from both chromophores according to their population evolution in equation (S28), considering the following relation between the radiative rate constants $\left(\frac{\kappa_{rad}^{Cy}}{\kappa_{rad}^{E-SAP}} = \frac{1}{4}\right)$, and a gaussian instrumental response function with $FWHM = 270\ fs$. The experimental Cy-SAP and IR-780 were scaled for comparison and are included to show that this simple kinetic model approaches the actual experimental observation (blue symbols). The Cy-SAP experimental trace (blue) decays in a somewhat shorter time scale (within 30% of the kinetic model). This is probably due to the fact that the kinetic model only considers a simple Förster type energy transfer with dipole-dipole coupling. Due to de small distance between the chromophores (R= 0.92 nm), it is expected that higher multipole interactions would accelerate the exciton migration).

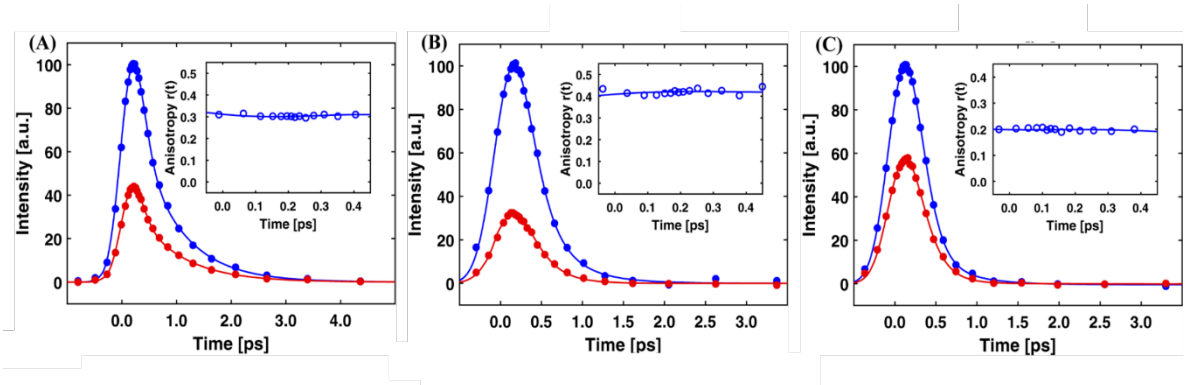

Figure S26. Time resolved emission at 525 nm with detection in the parallel (blue) and perpendicular orientation (red) with respect to the polarization of the 860 nm excitation pulses. (A) IR-780, (B) SAP and (C) Cy-SAP. The insets show the respective emission anisotropies $r = \frac{I_{\parallel} - I_{\perp}}{I_{\parallel} + 2I_{\perp}}$ near t=0. In the insets, the symbols correspond with the anisotropies calculated directly from the up-conversion data, and the solid line corresponds to the anisotropies calculated from the de-convoluted exponential fits to the parallel and perpendicular traces. Other emission wavelengths are presented below for each molecule in separate figures.

The time-resolved anisotropies were used to further demonstrate differences between the excited state evolution of each chromophore alone and of their dyad Cy-SAP. As can be seen, the anisotropies due to the excitation of the IR-780 system near t=0 correspond to a value of 0.3±0.03. For this cyanine-only case, the observed anisotropy is expected to be determined by the net effect of the transition dipole moments involved in the two-photon absorption, and their relative orientation with the transiently emissive cyanine S_2 state. Here, we note that the 0.3 anisotropy value is most likely due to the superposition of several available Sn, n>1 states at the respective two-photon energy in the initial excitation of IR-780 (see manuscript). The anisotropy values of the SAP solutions correspond to larger anisotropy values, of 0.42 ±0.03. this r(0) value is from the direct electronic excitation into the higher singlet states of the stilbenyl-azo system (which also may involve more than one state in the two-photon transition). Finally, the Cy-SAP anisotropy traces correspond with values of 0.1±0.03; a significantly smaller r(0) value in comparison with the IR-780 and SAP solutions (the IR780 and the Cy-SAP experiments were taken in back to back fashion in order to minimize small effects in the anisotropy results which can arise from small alignment differences). From the limited time resolution, it was not possible to reliably detect the time evolution of the anisotropies (due to the convoluted nature of the signals with the IRF). However, the difference in their near t=0 values are illustrative of the difference in the excited state properties of the three systems. The much lower anisotropy for Cy-SAP in comparison with the two separate systems indicates a rapid (comparable with our time resolution) evolution towards the SAP chromophore from the cyaninic chromophore.

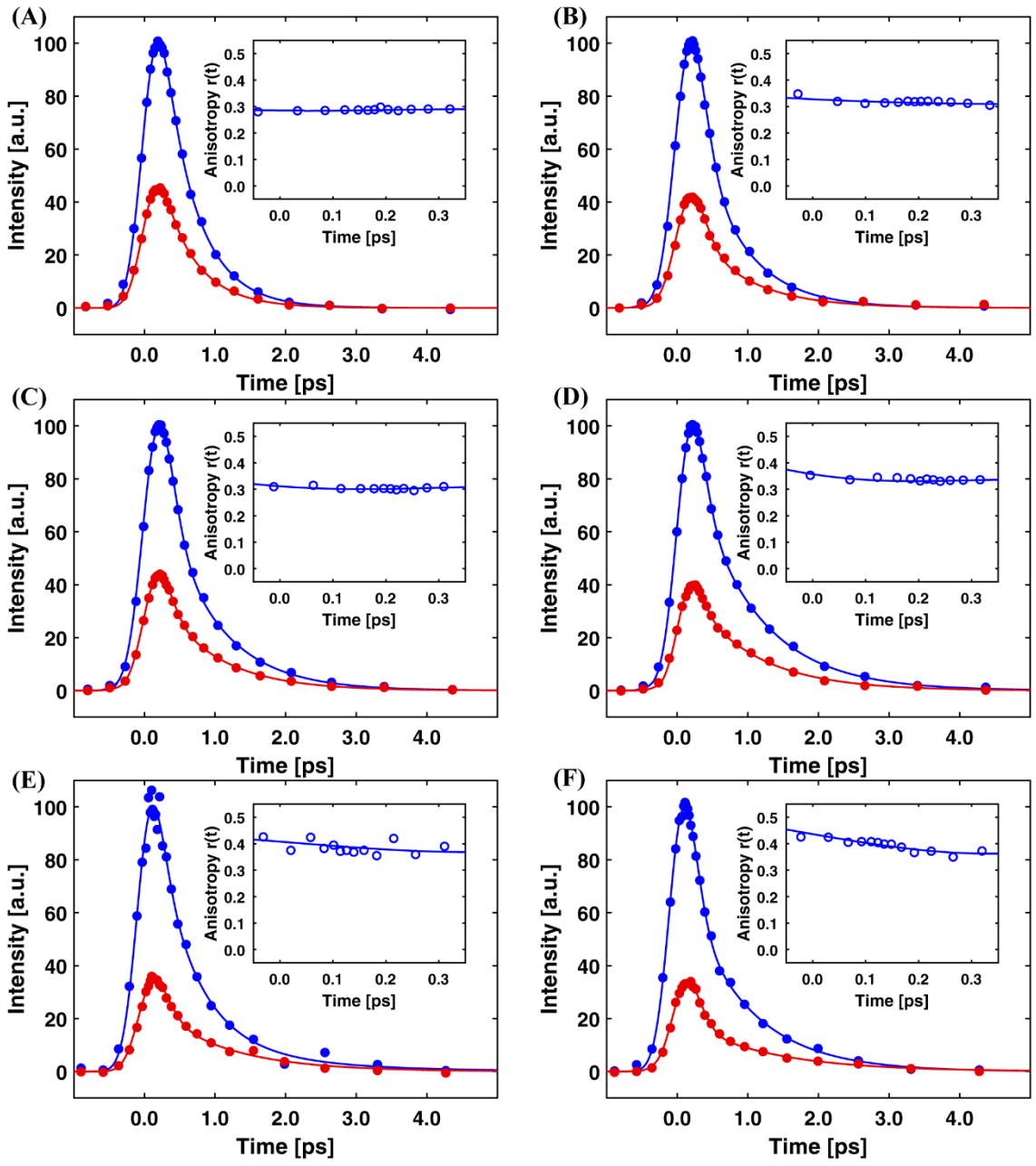

Figure S27. Main graphs: Femtosecond fluorescence up-conversion traces of IR-780 in acetonitrile solution detecting the parallel (blue) and perpendicular (red) emission polarization component of the fluorescence excitation with respect to the excitation polarization axis. The solid lines are fits to multiexponential decays convoluted with the instrument response function. The detections wavelengths were (A) 475 nm, (B) 500 nm, (C) 525 nm, (D) 575 nm, (E) 600 nm, (F) 625 nm, and the excitation wavelengths was 860 nm. The excitation is due to a two-photon absorption process. The inset shows the emission anisotropy values around t=0. The symbols are anisotropy values calculated with the experimental data, and the solid line was calculated considering the de-convoluted fits to the time resolved emission data.

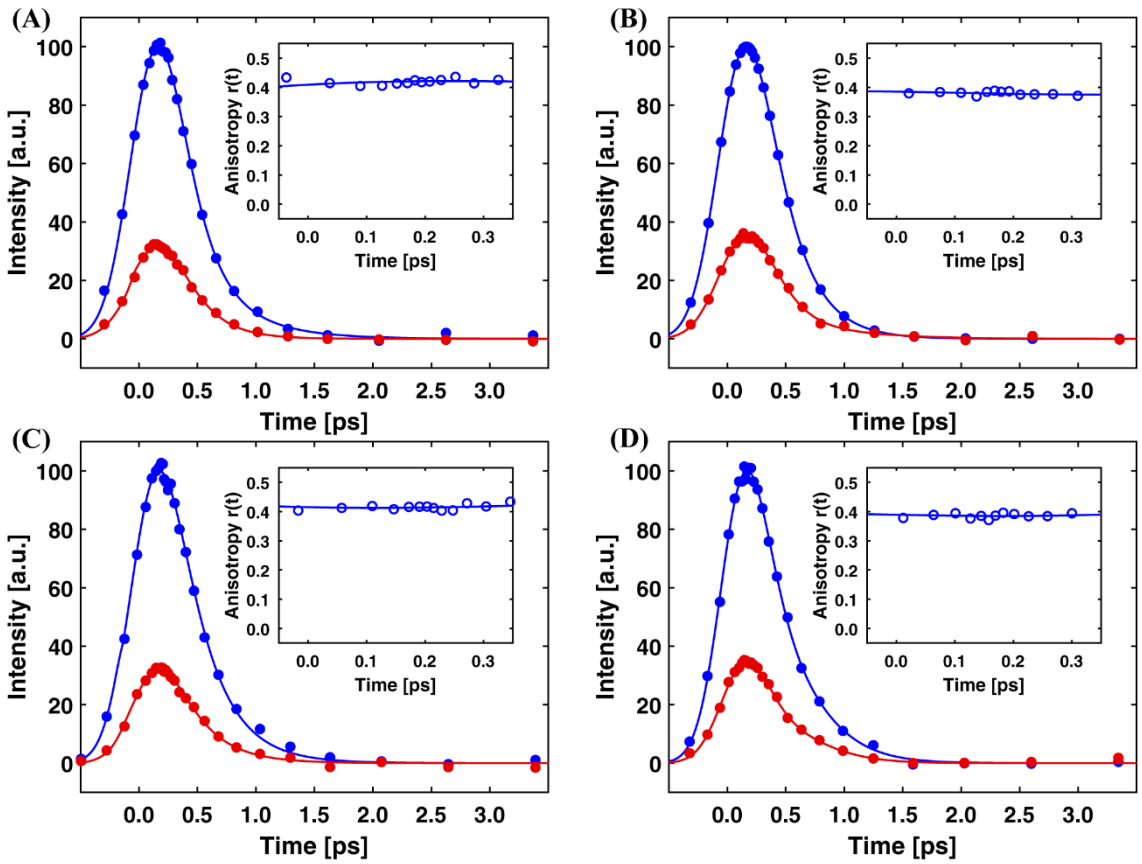

Figure S28. Main graph: Femtosecond fluorescence up-conversion traces of SAP in acetonitrile solution detecting the parallel (blue) and perpendicular (red) emission polarization component of the fluorescence excitation with respect to the excitation polarization axis. The solid lines are fits to multiexponential decays convoluted with the instrument response function. The detections wavelengths were (A**) 525 nm**, (B**) 550 nm**, (C) **575 nm**, (D) **600 nm**. and excitation wavelengths was 860 nm. The excitation is due to a two-photon absorption process. The inset shows the emission anisotropy values around t=0. The symbols are anisotropy values calculated with the experimental data, and the solid line was calculated considering the de-convoluted fits to the time resolved emission data.

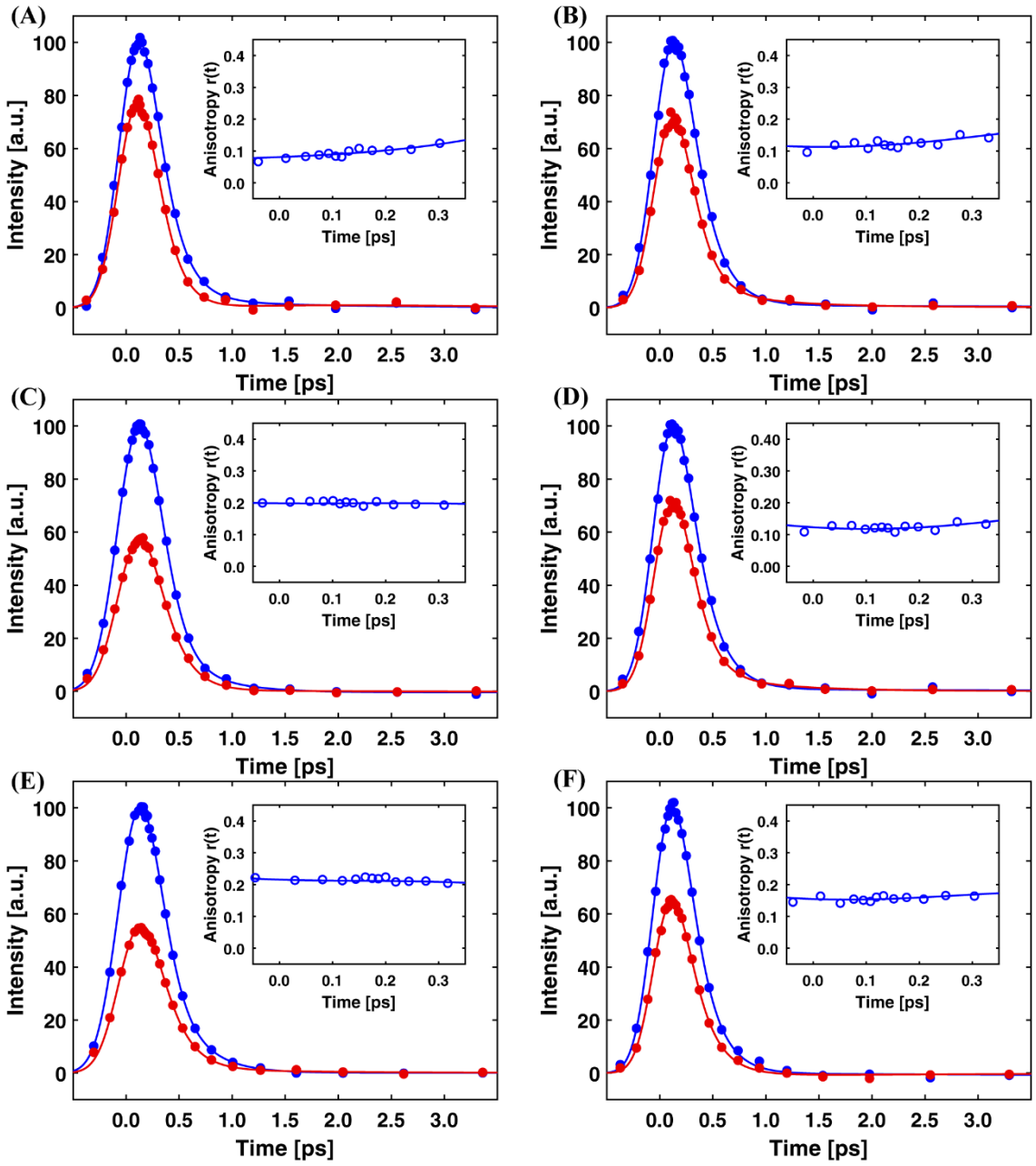

Figure S29. Main graph: Femtosecond fluorescence up-conversion traces of Cy-SAP in acetonitrile solution detecting the parallel (blue) and perpendicular (red) emission polarization component of the fluorescence excitation with respect to the excitation polarization axis. The solid lines are fits to multiexponential decays convoluted with the instrument response function. The detections wavelengths were (A) 475 nm, (B) 500 nm, (C) 525 nm, (D) 550 nm, (E) 575 nm, (F) 600 nm. and excitation wavelengths was 860 nm The excitation is due to a two-photon absorption process. The inset shows the emission anisotropy values around t=0. The symbols are anisotropy values calculated with the experimental data, and the solid line was calculated considering the de- convoluted fits to the time resolved emission data.

SAP Z-matrix (compact) coordinates ground state (using PBE0 functional).

0 1 (charge and multiplicity)

C						
C	1	1.39275				
C	1	1.39671	2	119.61700		
C	2	1.38551	1	119.66754	3	359.99093
C	3	1.38432	1	120.12180	2	0.00474
C	5	1.40321	3	121.40121	1	0.00601
H	2	1.08465	1	119.37131	3	179.99284
H	4	1.08626	2	119.01838	1	179.99507
H	3	1.08644	1	119.88643	2	180.01260
H	5	1.08480	3	118.31267	1	179.99160
O	1	1.35587	2	117.80485	3	179.99322
C	6	1.45743	5	123.75721	3	179.98418
H	12	1.08840	6	114.20916	5	180.13338
C	12	1.34662	6	126.94794	5	0.09769
H	14	1.08815	12	119.04262	6	359.93228
C	14	1.45637	12	126.57016	6	179.99678
C	16	1.40462	14	123.85884	12	359.31591
C	16	1.40794	14	118.61569	12	179.33418
C	17	1.38233	16	120.89334	14	179.96532
H	17	1.08464	16	120.28490	14	359.91376
C	18	1.38158	16	121.90957	14	180.03602
H	18	1.08655	16	118.77196	14	359.99913
C	19	1.40099	17	120.96156	16	0.02310
H	19	1.08540	17	120.60539	16	179.98720
H	21	1.08366	18	120.68576	16	179.96986
N	23	1.40145	19	115.95536	17	179.99380
N	26	1.26148	23	114.95763	19	180.14716
C	27	1.36315	26	115.80589	23	180.02714
C	28	1.39741	27	134.26613	26	0.12157
N	28	1.38092	27	117.79733	26	180.08868
C	29	1.39897	28	106.97546	27	179.98664
H	29	1.07929	28	125.17411	27	0.00181
C	30	1.35057	28	108.81585	27	180.00171
H	31	1.08013	29	127.24497	28	180.01605
H	33	1.07997	30	120.75943	28	180.00690
C	30	1.44995	28	125.56018	27	0.10853
H	36	1.09077	30	110.50276	28	300.20511
H	36	1.09089	30	110.54866	28	60.94477
H	36	1.08924	30	108.29506	28	180.58173
H	11	0.96219	1	109.98463	2	180.00183

Ground state energy E(PBE0) = -972.80297702 Hartrees.

SAP Z-matrix (compact) coordinates ground state (using M06 functional).

0 1 (charge and multiplicity)

C						
C	1	1.39041				
C	1	1.39417	2	119.71747		
C	2	1.38312	1	119.62763	3	0.03132
C	3	1.38208	1	120.06896	2	359.97672
C	5	1.40073	3	121.34589	1	359.92103
H	2	1.08542	1	119.16926	3	180.05741
H	4	1.08729	2	119.21135	1	179.99537
H	3	1.08710	1	119.71912	2	179.89821
H	5	1.08602	3	118.48462	1	179.82563
O	1	1.35468	2	117.74693	3	179.93751
C	6	1.45549	5	123.54079	3	180.15386
H	12	1.09045	6	114.26330	5	181.50606
C	12	1.34294	6	126.95505	5	1.72013
H	14	1.09021	12	119.01566	6	0.26344
C	14	1.45459	12	126.49413	6	180.05437
C	16	1.40221	14	123.61402	12	1.15300
C	16	1.40529	14	118.73335	12	181.07463
C	17	1.37989	16	120.80652	14	180.04296
H	17	1.08577	16	120.19846	14	0.15711
C	18	1.37946	16	121.85589	14	179.89811
H	18	1.08756	16	118.64532	14	359.90290
C	19	1.39864	17	120.93909	16	0.05397
H	19	1.08635	17	120.80589	16	180.03088
H	21	1.08459	18	120.73901	16	179.99966
N	23	1.40372	19	115.84867	17	179.94842
N	26	1.26158	23	114.95111	19	181.18332
C	27	1.36434	26	115.59595	23	180.14690
C	28	1.39377	27	134.14766	26	0.43503
N	28	1.38239	27	117.90026	26	180.39541
C	29	1.39781	28	107.07024	27	179.97661
H	29	1.07997	28	125.07819	27	0.01905
C	30	1.35210	28	108.62314	27	180.00353
H	31	1.08026	29	127.19046	28	180.02257
H	33	1.08087	30	120.58815	28	180.03097
C	30	1.45029	28	125.60567	27	0.07610
H	36	1.09186	30	110.64982	28	299.54439
H	36	1.09184	30	110.64305	28	60.22476
H	36	1.09021	30	108.37246	28	179.88591
H	11	0.96346	1	110.32792	2	180.03584

Ground state energy E(M06) = -973.22349353 Hartrees.

Cy Z-matrix (compact) coordinates ground state (using PBE0 functional).

1 1 (charge and multiplicity)

C						
C	1	1.51821				
C	1	1.51788	2	110.65443		
H	1	1.09623	2	109.33109	3	239.44156
H	1	1.09337	2	110.15449	3	121.98894
C	3	1.50982	1	112.21427	2	306.63605
H	3	1.09347	1	109.49676	2	185.05193
H	3	1.09869	1	109.85507	2	68.48147
C	2	1.50955	1	111.99773	3	54.26578
H	2	1.09860	1	109.84180	3	292.45848
H	2	1.09332	1	109.53386	3	175.81852
C	9	1.39534	2	120.67837	1	155.14152
C	12	1.39265	9	125.49262	2	2.00180
C	13	1.39138	12	124.91914	9	179.85552
N	14	1.34988	13	122.28586	12	179.18883
C	14	1.52886	13	128.75147	12	359.06037
C	15	1.40276	14	111.54875	13	178.49825
C	17	1.39086	15	108.92674	14	1.30977
C	17	1.38750	15	128.67946	14	181.24344
C	19	1.39391	17	117.11953	15	180.49670
C	20	1.39274	19	121.22284	17	359.91525
C	18	1.38243	17	119.99536	15	179.43775
C	16	1.53780	14	111.61582	13	63.84735
H	23	1.09267	16	110.96204	14	53.61914
H	23	1.09147	16	111.85386	14	292.43266
H	23	1.09298	16	109.23192	14	172.89374
C	16	1.53760	14	111.84264	13	298.02035
H	27	1.09266	16	110.94327	14	306.68324
H	27	1.09309	16	109.18158	14	187.49128
H	27	1.09137	16	111.95147	14	67.95384
C	15	1.45477	14	125.80111	13	0.42561
C	31	1.52518	15	112.86662	14	86.84467
H	31	1.09257	15	108.38837	14	323.36127
H	31	1.09255	15	107.33925	14	208.93203
C	32	1.52129	31	111.43782	15	179.65183
H	32	1.09521	31	108.98626	15	57.80935
H	32	1.09521	31	109.14441	15	301.65081
H	35	1.09448	32	111.25457	31	300.03548
H	35	1.09262	32	110.79529	31	180.18136
H	35	1.09451	32	111.28093	31	60.29432
H	19	1.08372	17	122.29760	15	0.80811
H	20	1.08478	19	119.09725	17	180.03380
H	21	1.08457	20	119.70858	19	179.99672
H	22	1.08557	18	121.04601	17	180.16280
H	6	4.97069	3	120.13779	1	233.26248
H	45	1.77161	6	44.63559	3	179.01638
C	46	1.09138	45	35.81594	6	115.86260
H	47	1.09304	46	108.00311	45	117.09124
H	7	3.58132	3	151.67535	1	158.71484
H	49	2.52152	7	86.09389	3	117.81130
H	50	1.76679	49	68.70750	7	140.06348
C	51	1.09262	50	36.15186	49	65.19510
C	49	1.09522	7	129.68615	3	74.34046

C	47	2.53998	46	96.56524	45	268.66354
C	6	1.39563	3	120.52319	1	202.86042
C	54	1.52860	47	34.16559	46	239.91856
H	53	2.17249	49	95.32376	7	339.75133
N	54	1.34977	47	121.47269	46	162.81410
C	56	1.51041	54	101.31990	47	242.80838
C	57	1.09257	53	40.92085	49	238.29239
C	59	1.39087	56	109.22588	54	359.51612
C	59	1.38244	56	130.77088	54	179.58659
C	54	1.39154	47	107.91839	46	13.92867
H	53	1.09523	49	106.68567	7	197.14850
H	62	1.08559	59	121.05180	56	0.04250
C	61	1.38755	59	122.38962	56	179.62532
C	62	1.39667	59	118.70167	56	180.12585
H	52	1.09447	51	107.75102	50	116.11592
C	67	1.39276	62	120.56148	59	0.06234
C	56	1.53805	54	111.56561	47	125.78146
H	70	1.09145	56	111.85503	54	292.37552
H	66	1.08376	61	122.30037	59	180.66231
H	67	1.08456	62	119.73526	59	179.91724
H	70	1.09297	56	109.19288	54	172.85160
H	69	1.08479	67	119.67744	62	179.74935
H	60	1.09253	57	106.28053	53	239.61162
H	70	1.09268	56	110.95437	54	53.58288
H	55	1.08150	6	116.44668	3	180.03631
H	63	1.08328	54	116.84677	47	147.46501
H	12	1.08150	9	116.40635	2	180.93828
H	13	1.08337	12	118.22432	9	0.86040
C	6	1.40597	3	117.74950	1	24.96425
Cl	82	1.75600	6	117.59608	3	182.07165

Ground state energy E(PBE0) = -1966.32558585 Hartrees

Cy Z-matrix (compact) coordinates ground state (using M06 functional).

1 1 (charge and multiplicity)

C						
C	1	1.51529				
C	1	1.51510	2	110.41455		
H	1	1.09824	2	109.30551	3	239.64751
H	1	1.09414	2	110.35288	3	122.23605
C	3	1.50773	1	112.07547	2	306.07151
H	3	1.09516	1	109.81199	2	184.33232
H	3	1.10086	1	109.81979	2	67.82267
C	2	1.50749	1	111.92493	3	54.71481
H	2	1.10079	1	109.81327	3	292.96737
H	2	1.09501	1	109.80849	3	176.41370
C	9	1.39090	2	120.67262	1	155.65717
C	12	1.39035	9	126.43989	2	2.06775
C	13	1.38814	12	123.79245	9	178.70022
N	14	1.34994	13	122.71383	12	179.04147
C	14	1.52765	13	128.39144	12	358.64558
C	15	1.40555	14	111.47171	13	177.62510
C	17	1.38784	15	108.86855	14	1.74109
C	17	1.38440	15	128.65383	14	181.76703
C	19	1.39214	17	117.05419	15	180.43181
C	20	1.39060	19	121.21862	17	359.91021
C	18	1.37994	17	120.02351	15	179.47316
C	16	1.53315	14	111.66545	13	64.92546
H	23	1.09459	16	110.87184	14	52.40344
H	23	1.09361	16	112.19997	14	291.06221
H	23	1.09460	16	109.22941	14	171.48013
C	16	1.53263	14	112.15760	13	298.73083
H	27	1.09454	16	110.86342	14	308.07019
H	27	1.09464	16	109.13575	14	189.08894
H	27	1.09337	16	112.38656	14	69.55067
C	15	1.45571	14	126.07866	13	0.67722
C	31	1.51973	15	112.36247	14	88.33861
H	31	1.09445	15	108.68666	14	324.80889
H	31	1.09542	15	107.48705	14	210.32468
C	32	1.51633	31	111.03648	15	179.23920
H	32	1.09750	31	108.93020	15	57.26309
H	32	1.09738	31	109.11292	15	301.41712
H	35	1.09552	32	111.06837	31	300.22209
H	35	1.09269	32	111.34617	31	180.11978
H	35	1.09555	32	111.08603	31	59.99079
H	19	1.08496	17	122.16959	15	0.76199
H	20	1.08523	19	119.16183	17	180.04910
H	21	1.08503	20	119.66249	19	180.01937
H	22	1.08703	18	120.95983	17	180.11225
H	6	4.90525	3	121.23909	1	234.00445
H	45	1.77443	6	44.96414	3	177.84376
C	46	1.09333	45	35.82813	6	115.75664
H	47	1.09462	46	107.78954	45	116.83773
H	7	3.77427	3	150.03440	1	156.84748
H	49	2.52317	7	86.76196	3	118.96300
H	50	1.76774	49	69.04383	7	142.56637
C	51	1.09271	50	36.16787	49	64.82340
C	49	1.09740	7	128.32390	3	74.01352

C	47	2.53917	46	97.77621	45	268.90792
C	6	1.39080	3	120.52315	1	202.84598
C	54	1.52753	47	33.98217	46	241.00480
H	53	2.17031	49	95.15371	7	342.73824
N	54	1.35004	47	121.46368	46	164.20839
C	56	1.50802	54	101.39086	47	243.01551
C	57	1.09444	53	40.75818	49	238.12620
C	59	1.38795	56	109.37210	54	359.36278
C	59	1.37973	56	130.53739	54	179.35492
C	54	1.38820	47	107.55236	46	14.82503
H	53	1.09749	49	106.46407	7	200.33981
H	62	1.08698	59	120.97983	56	0.14098
C	61	1.38457	59	122.40811	56	179.47109
C	62	1.39450	59	118.63039	56	180.25820
H	52	1.09555	51	107.75746	50	115.89632
C	67	1.39054	62	120.56244	59	0.08189
C	56	1.53342	54	111.74154	47	126.23095
H	70	1.09359	56	112.26450	54	290.94083
H	66	1.08491	61	122.18525	59	180.72861
H	67	1.08503	62	119.77892	59	179.89435
H	70	1.09459	56	109.16047	54	171.38969
H	69	1.08524	67	119.61895	62	179.69773
H	60	1.09544	57	106.11640	53	239.52688
H	70	1.09460	56	110.87188	54	52.34588
H	55	1.08123	6	116.14587	3	180.06914
H	63	1.08565	54	117.53154	47	147.64028
H	12	1.08144	9	116.14164	2	180.85614
H	13	1.08572	12	118.77442	9	359.95236
C	9	1.40339	2	117.59612	1	333.19486
Cl	82	1.76636	9	117.68096	2	178.86214

Ground state energy E(M06) = -1966.97522035 Hartrees

References

1. Hochberger-Roa, F. *et al.* Synthesis and Catalytic Applications of [N,N]-Pyrrole Ligands for the Regioselective Synthesis of Styrene Derivatives. *Adv. Synth. Catal.* **361**, 4055–4064 (2019).
2. Rodríguez-Córdoba, W., Noria, R., Guarín, C. A. & Peon, J. Ultrafast photosensitization of phthalocyanines through their axial ligands. *J. Am. Chem. Soc.* **133**, 4698–4701 (2011).
3. Rodríguez-Córdoba, W., Sierra, C. A., Ochoa Puentes, C., Lahti, P. M. & Peon, J. Photoinduced energy transfer in bichromophoric pyrene-PPV oligomer systems: The role of flexible donor-acceptor bridges. *J. Phys. Chem. B* **116**, 3490–3503 (2012).
4. Gutiérrez-Arzaluz, L., López-Arteaga, R., Cortés-Guzmán, F. & Peon, J. Nitrated Fluorophore Formation upon Two-Photon Excitation of an Azide with Extended Conjugation. *J. Phys. Chem. B* **121**, 9910–9919 (2017).
5. Gutiérrez-Arzaluz, L., Guarin, C. A., Rodríguez-Córdoba, W. & Peon, J. Dynamics of the formation of a charge transfer state in 1,2-bis(9-anthryl)acetylene in polar solvents: Symmetry reduction with the participation of an intramolecular torsional coordinate. *J. Phys. Chem. B* **117**, 12175–12183 (2013).
6. Fulmer, G. R. *et al.* NMR chemical shifts of trace impurities: Common laboratory solvents, organics, and gases in deuterated solvents relevant to the organometallic chemist. *Organometallics* **29**, 2176–2179 (2010).
7. Frisch, M. J. *et al.* Gaussian 09, Revision E.01. (2009).
8. Andzelm, J. *et al.* Performance of DFT methods in the calculation of optical spectra of TCF-chromophores. *J. Chem. Theory Comput.* **5**, 2835–2846 (2009).
9. Jacquemin, D., Perpète, E. A., Ciofini, I. & Adamo, C. Assessment of functionals for TD-DFT calculations of singlet-triplet transitions. *J. Chem. Theory Comput.* **6**, 1532–1537 (2010).
10. Jacquemin, D., Brémond, E., Planchat, A., Ciofini, I. & Adamo, C. TD-DFT vibronic couplings in anthraquinones: From basis set and functional benchmarks to applications for industrial dyes. *J. Chem. Theory Comput.* **7**, 1882–1892 (2011).
11. Bousquet, D. *et al.* Excited-state geometries of heteroaromatic compounds: A comparative TD-DFT and SAC-CI study. *J. Chem. Theory Comput.* **9**, 2368–2379 (2013).
12. Jacquemin, D., Perpète, E. A., Scuseria, G. E., Ciofini, I. & Adamo, C. TD-DFT performance for the visible absorption spectra of organic dyes: Conventional versus long-range hybrids. *J. Chem. Theory Comput.* **4**, 123–135 (2008).
13. Bousquet, D. *et al.* Benchmark study on the triplet excited-state geometries and phosphorescence energies of heterocyclic compounds: Comparison between TD-PBE0 and SAC-CI. *J. Chem. Theory Comput.* **10**, 3969–3979 (2014).
14. Jacquemin, D., Wathelet, V., Perpète, E. A. & Adamo, C. Extensive TD-DFT benchmark: Singlet-excited states of organic molecules. *J. Chem. Theory Comput.* **5**, 2420–2435 (2009).
15. Ravelli, D., Dondi, D., Fagnoni, M., Albini, A. & Bagno, A. Predicting the UV spectrum of polyoxometalates by TD-DFT. *J. Comput. Chem.* **32**, 2983–2987 (2011).
16. Cooper, J. K., Grant, C. D. & Zhang, J. Z. Experimental and TD-DFT study of optical absorption of six explosive molecules: RDX, HMX, PETN, TNT, TATP, and HMTD. *J. Phys. Chem. A* **117**, 6043–6051 (2013).
17. Taniguchi, M., Du, H. & Lindsey, J. S. PhotochemCAD 3: Diverse Modules for Photophysical Calculations with Multiple Spectral Databases. *Photochem. Photobiol.* **94**, 277–289 (2018).
18. Calbo, J. *et al.* Tuning Azoheteroarene Photoswitch Performance through Heteroaryl Design. *J. Am. Chem. Soc.* **139**, 1261–1274 (2017).
19. Rodríguez-Romero, J. *et al.* Fluorophore Release from a Polymethinic Photoremovable Protecting Group Through a Nonlinear Optical Process. *ChemPhotoChem* **1**, 397–407 (2017).
20. Muñoz-Rugeles, L. *et al.* Synthesis and Photodynamics of Stilbenyl-Azopyrroles: Two-Photon Controllable Photoswitching Systems. *ChemPhotoChem* **4**, 144–154 (2020).

Author Contributions

Emmanuel Villatoro, Leonardo Muñoz-Rugeles, Jesús Durán-Hernández, Bernardo Salcido, Nuria Esturau-Escofet: investigation and formal analysis.

Jose G. López-Cortés, M. Carmen Ortega-Alfaro and Jorge Peón: Investigation, project administration, validation, manuscript writing, funding acquisition.